DOE/ER/13777-12

PREDICTION OF THERMODYNAMIC PROPERTIES OF COMPLEX FLUIDS

Marc D. Donohue
The Johns Hopkins University
Department of Chemical Engineering
Baltimore, Maryland 21218

Final Report

Prepared for:
CHEMICAL SCIENCES DIVISION
OFFICE OF BASIC ENERGY SCIENCES
U.S. DEPARTMENT OF ENERGY

Agreement # DE-FG02-87ER13777-A014

ABSTRACT

The goal of this research has been to generalize Density Functional Theory (DFT) for complex molecules, i.e. molecules whose size, shape, and interaction energies cause them to show significant deviations from mean-field behavior. We considered free energy functionals and minimized them for systems with different geometries and dimensionalities including confined fluids (such as molecular layers on surfaces and molecules in nano-scale pores), systems with directional interactions and order-disorder transitions, amphiphilic dimers, block copolymers, and self-assembled nano-structures. The results of this procedure include equations of equilibrium for these systems and the development of computational tools for predicting phase transitions and self-assembly in complex fluids.

DFT was developed for confined fluids. A new phenomenon, surface compression of confined fluids, was predicted theoretically and confirmed by existing experimental data and by simulations. The strong attraction to a surface causes adsorbate molecules to attain much higher densities than that of a normal liquid. Under these conditions, adsorbate molecules are so compressed that they repel each other. This phenomenon is discussed in terms of experimental data, results of Monte Carlo simulations, and theoretical models. Lattice version of DFT was developed for modeling phase transitions in adsorbed phase including wetting, capillary condensation, and ordering.

Phase behavior of amphiphilic dimers on surfaces and in solutions was modeled using lattice DFT and Monte Carlo simulations. This study resulted in predictive models for adsorption isotherms and for local density distributions in solutions. We have observed a wide variety of phase behavior for amphiphilic dimers, including formation of lamellae and micelles.

Block copolymers were modeled in terms of configurational probabilities and in the approximation of random mixing entropy. Probabilities of different orientations for the segments were considered as order parameters and the free energy was written as a functional of these parameters. Imposing boundary conditions allowed us to apply this approach to confined fluids.

Equilibrium self-assembly in fluids was studied in the framework of the lattice density functional theory (DFT). In particular, DFT was used to model the phase behavior of anisotropic monomers. Though anisotropic monomers are a highly idealized model system, the analysis presented here demonstrates a formalism that can be used to describe a wide variety of phase transitions, including processes referred to as self-assembly. In DFT, the free energy is represented as a functional of order parameters. Minimization of this functional allows modeling spontaneous nano-scale phase transitions and self-assembly of supramolecular structures. In particular, this theory predicts micellization, lamellization, fluid – glass phase transitions, crystallization, and more.

A classification of phase transitions based on general differences in self-assembled structures is proposed. The roles of dimensionality and intermolecular interactions in different types of phase transitions are analyzed. The concept of “genetic” codes is discussed in terms of structural variety of self-assembled systems.

Confined Fluids

Adsorption in Nano-Porous Systems

Here we consider vapor adsorption in slit pores using the Ono-Kondo version of lattice Density Functional Theory. In this model, the lattice contains adsorbate molecules and vacancies. There are interactions between nearest neighbors with ε being the energy of adsorbate - adsorbate interactions, and ε_S being the energy for adsorbate - surface interactions. For attractive interactions, ε and ε_S are negative, and for repulsive interactions they are positive. We assume that the slit walls are two flat boundaries which are identical and that the width of the slit is divided into N layers.

The general form of the equation of equilibrium for this case can be represented in the following form [1, 2]:

$$(1/x_b)\ln\{[x_a (1 - x_b)]/[H(1 - x_a)x_b]\} + (k_1 \varepsilon x_a /x_b + k_2 \varepsilon)/kT = 0 \qquad (1)$$

which relates the normalized density in the bulk, x_b , to the normalized density in adsorbed phase, x_a . In this equation,

$$H = \exp(-k_0 \varepsilon_s /kT) \qquad (2)$$

and k_0 , k_1 ,and k_2 are constants depending on the geometry of the lattice.

As seen from equation (1), plotting

$$Y = (1/x_b)\ln\{[x_a (1 - x_b)]/[H(1 - x_a)x_b]\}$$

versus x_a /x_b allows one to obtain information about intermolecular interactions in the adsorbed layer. In particular, the sign in the slope of this line allows one to conclude whether the interactions are attractive or repulsive. Figure 1 gives an example of the experimental isotherm for nitrogen in activated carbon plotted in the proposed coordinates. As seen from Figure 1 (lower plate), the slope of the line is negative, indicating strong repulsions of nitrogen molecules in the adsorbed phase [2]. This work is described further in the paper "Vapor adsorption on microporous adsorbents" that appeared in *Carbon*, v.38, p. 701-708 (2000) and in the paper "Intermolecular repulsions in adsorbed layers" that has been published in *Journal of Colloid and Interface Science*, v.227, p. 553-560 (2000).

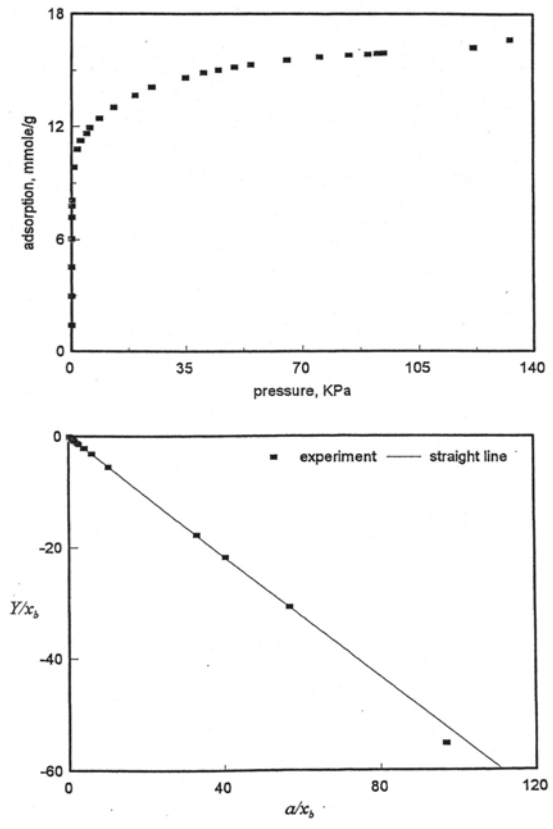

Figure 1. Adsorption isotherm for nitrogen on activated carbon at T = 90 K. Data from [3]. The upper graph shows adsorption isotherm in standard coordinates; the lower graph is the isotherm in coordinates of equation (1).

The behavior of this and other data in these coordinates led to the discovery of a new phenomenon, surface compression of adsorbates for gases adsorbed on solids. The strong attraction to a surface causes adsorbate molecules to attain much higher densities than that of a normal liquid. Under these conditions, adsorbate molecules are so compressed that they repel each other. This phenomenon is discussed in terms of experimental data, results of Monte Carlo simulations, and theoretical models.

An approximate model for monolayer adsorption of Lennard-Jones molecules on a surface was derived. This model predicts adsorbate-adsorbate repulsions for strong adsorbate-adsorbent interactions. This model is applicable to both monolayer adsorption and to the first layer in multilayer adsorption. A linear form of this new model allows one to determine the adsorbate - adsorbate interaction energy in the adsorbed layer from experimental data:

$$\ln\frac{(a/a_m)(1-x_b)}{(1-a/a_m)x_b}+\frac{\varphi_s}{kT}+\frac{\lambda a\varphi(r^*)}{kT}-\frac{\lambda' x_b\varphi(r^{*'})}{kT}=0 \qquad (3)$$

where a is the adsorption amount, a_m is the maximum density of adsorbate molecules (per square meter) that can be on the surface (i.e. the monolayer capacity), x_b is the density of adsorbate molecules in the bulk (far from the surface), φ_s is an average energy of the molecule-surface interaction, φ is the Lennard-Jones potential function, r^* and $r^{*'}$ are the distances between molecules in two-dimensional and three-dimensional liquid respectively. Here λ, λ', are constants. In equation (3), the first two terms dominate and can be combined to:

$$Y=\ln\frac{(a/a_m)(1-x_b)}{(1-a/a_m)x_b\exp(-\varphi_s/kT)} \qquad (4)$$

Figure 2 shows experimental isotherms for adsorption of various vapors on different adsorbents in coordinates of equation (3) (Y versus a/x_b). As shown by Figure 2, in these coordinates, experimental data are straight lines near monolayer coverage (at small a/x_b). An interesting thing is that the slope of the straight lines in Figure 2 is negative which indicates positive $\varphi(r^*)$. So, in all these cases, there is a repulsion between molecules in adsorbed layer near monolayer coverage.

Analysis of different systems (such as nitrogen, carbon dioxide, hydrocarbons on various adsorbents) shows that the energies of molecule - molecule interactions in the adsorbed phase near monolayer coverage are positive, indicating adsorbate-adsorbate repulsions, and, hence, that the adsorbates are compressed fluids [12]. This should be taken into account in the analysis of equations of state for the adsorbed phase and in using adsorption to characterize porous materials. It also should have an effect on solidification of the adsorbed layer and on the rates of reaction on catalyst surfaces. The results presented here also show that the concept of “monolayer capacity” needs revision because it is a function of the adsorbate-adsorbent interaction energy.

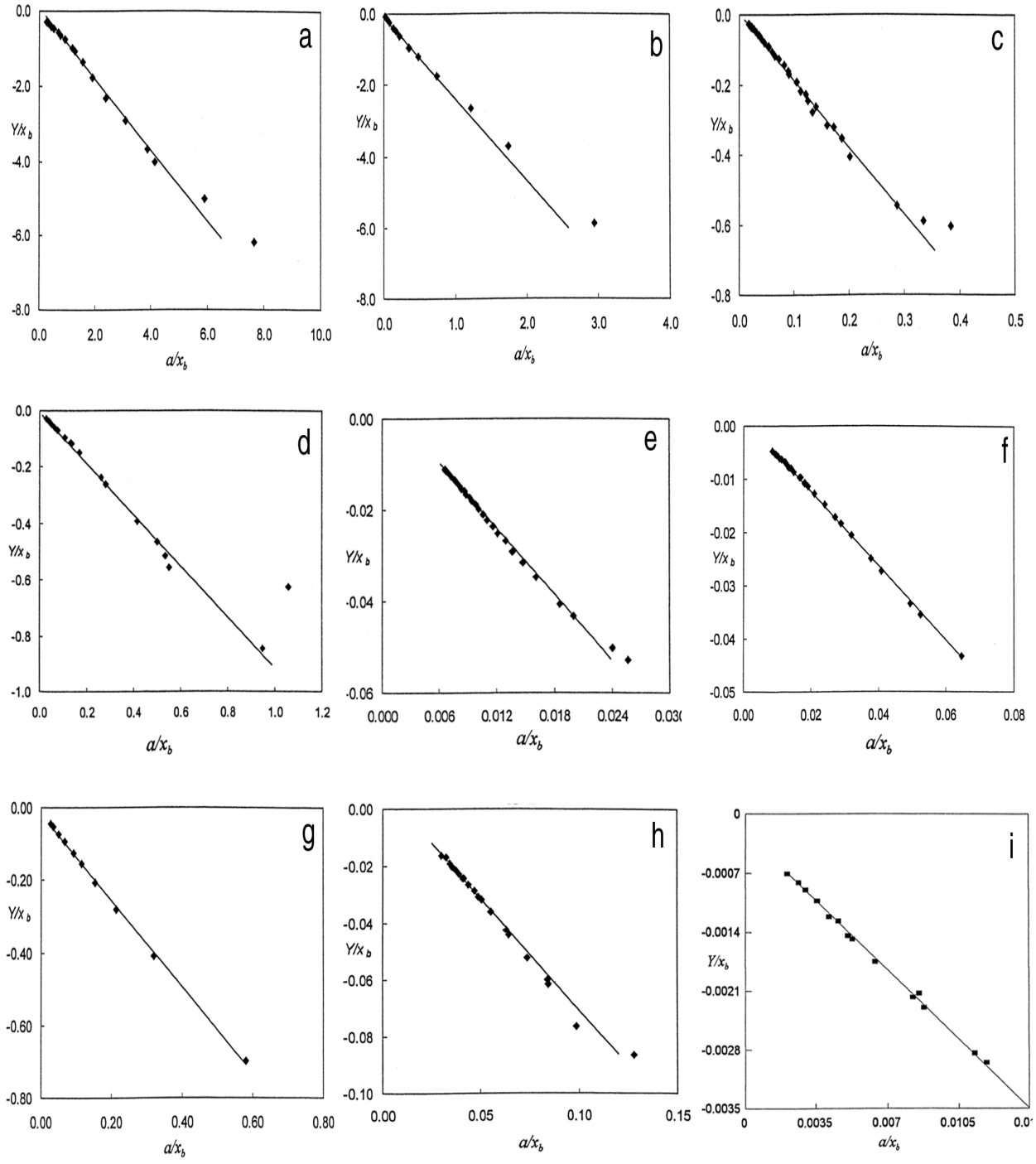

Figure 2. Adsorption isotherms for different systems in coordinates of equation (3).
a: benzene on silica gel at T = 303 K; data from [4];
b: butane on carbon molecular sieve at T = 324 K; data from [5];
c: carbon dioxide on h-mordenite at T = 303 K; data from [6];
d: carbon dioxide on zeolite molecular sieve at T = 298 K; data from [7];
e: carbon monoxide on zeolite at T = 228 K; data from [8];

f: ethylene on activated carbon at T = 311 K; data from [9];
g: ethylene on carbon molecular sieve at T = 279 K; data from [5];
h: acetylene on activated carbon at T = 293 K; data from [10];
i: methane on activated carbon at T = 213 K; data from [11].

This work is described further in the paper "Surface Compression in Adsorption Systems" that appeared in *Colloids and Surfaces A*, v.187-188, p. 95-108 (2001).

Density Functional Theory for Molecules in Nano-Scale Pores

Here, we present an analysis of adsorption behavior in slit-like pores using density functional theory (DFT) for a confined lattice [13]. Consider molecules of one-component gas on a lattice with two boundaries (walls). There are interactions between nearest neighbors with ε being the energy for adsorbate - adsorbate interactions, and ε_S being the energy for adsorbate - surface interactions.

Figure 3 shows the adsorption isotherm obtained from the DFT calculations [14] at $\varepsilon/kT = -1.0$ and $\varepsilon_s/kT = -3.0$ for 20 layer slit-like pore. As shown in Figure 3, there are three steps: step one is the two-dimensional condensation in the first layer (wetting phase transition); step 2 is another two-dimensional phase transition in the second layer; and step 3 is the capillary condensation of all other layers. Dotted line 4 shows the point of the three-dimensional condensation. As seen from Figure 3, the capillary condensation occurs at the density slightly lower than the equilibrium bulk condensation.

The DFT approach allows predictions of the adsorption behavior not only for pure components, but also for mixtures of molecules in nano-scale pores. In this case, the lattice DFT considers energies of interactions for all types of molecules; say, for the mixture of A and B molecules, these energies are ε_{AA}, ε_{AB}, ε_{BB} , ε_{AS} ,ε_{BS} .

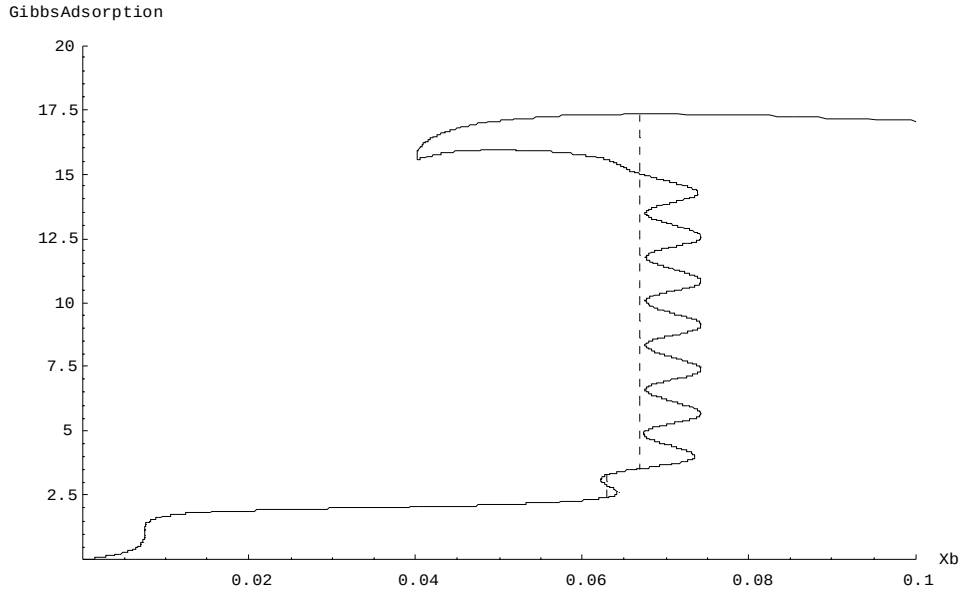

Figure 3. The adsorption isotherm obtained from the DFT calculations [14] at $\varepsilon/kT = -1.0$ and $\varepsilon_s/kT = -3.0$ for 20 layer slit-like pore.

This work is described in more detail in the paper "Phase loops in density-functional-theory calculations of adsorption in nanoscale pores" that appeared in *Physical Review E*, v.60, p.5552-5560 (1999).

Amphiphilic Dimers on Surface

For amphiphilic dimers adsorbed at a surface, there are three configurations in the layer adjacent to the surface [15]. The first configuration is to have the dimer molecules perpendicular to the surface with "***A***" segments in the first layer and "***B***" segments in the second layer. The fraction of sites occupied by molecules of this configuration in the first layer is represented by $x^A_{\perp,1}$. Similarly, if we have a dimer that is perpendicular to the surface, but with "***B***" segments in the first layer and "***A***" segments in the second layer, we have the second type of configuration. The segmental density of sites occupied by molecules of this configuration in the first layer is represented by $x^B_{\perp,1}$. The third configuration is to have both "***A***" and "***B***" segments in the first layer. The segmental density of "***A***" segments in this configuration, $x^A_{//,1}$, is equal to the segmental density of "***B***" segments in this configuration, $x^B_{//,1}$, and therefore this will be denoted as $x_{//,1}$.

Minimization of free energy for this system gives a set of equations of equilibrium that relate the density of segments in each layer to the segmental densities in adjacent layers and in the bulk [15, 16]. In particular, for the first layer, the equation of equilibrium for the parallel configuration is:

$$\ln\{[2/4\, x_{//,1}(1-x_4)^2]/[(1-x_1)^2(x_4/12)]\} + (\varepsilon_{AS}+\varepsilon_{BS})/kT + [3(x^A_1 - \tfrac{1}{4}x^A_{//,1}) + (x^A_2 - x^B_{\perp,1}) - 25/6\, x^A_4]\,\varepsilon_{AA}/kT + [3(x^B_1 - \tfrac{1}{4}x^B_{//,1}) + (x^B_2 - x^A_{\perp,1}) - 25/6\, x^B_4]\,\varepsilon_{BB}/kT \quad 3(x^A_1 - \tfrac{1}{4}x^A_{//,1}) + (x^A_2 - x^B_{\perp,1}) + 3(x^B_1 - \tfrac{1}{4}x^B_{//,1}) + (x^B_2 - x^A_{\perp,1}) - 25/6\, x_4]\,\varepsilon_{AB}/kT = 0 \qquad (5)$$

For layer j, the equations of equilibrium for perpendicular and parallel configurations are:

$$\ln\{[x^A_{\perp,j}(1-x_4)^2]/[(1-x_j)(1-x_{j+1})(x^A_4/6)]\} + [(x^A_{j-1} - x^A_{\perp,j-1}) + 4(x^A_j - \tfrac{1}{4}x^A_{//,j}) - 25/6\, x^A_4]\,\varepsilon_{AA}/kT + [4(x^B_{j+1} - \tfrac{1}{4}x^B_{//,j+1}) + (x^B_{j+2} - x^A_{\perp,j+1}) - 25/6\, x^B_4]\varepsilon_{BB}/kT + (x^B_{j-1} - x^B_{\perp,j-1}) + 4(x^B_j - \tfrac{1}{4}x^B_{//,j}) + 4(x^A_{j+1} - \tfrac{1}{4}x^A_{//,j+1}) + (x^A_{j+2} - x^B_{\perp,j+1})]\,\varepsilon_{AB}/kT = 0 \qquad (6)$$

$$\ln\{[x^B_{\perp,j}(1-x_4)^2]/[(1-x_j)(1-x_{j+1})(x^B_4/6)]\} + [(x^B_{j-1} - x^B_{\perp,j-1}) + 4(x^B_j - \tfrac{1}{4}x^B_{//,j}) - 25/6\, x^B_4]\varepsilon_{BB}/kT + [4(x^A_{j+1} - \tfrac{1}{4}x^A_{//,j+1}) + (x^A_{j+2} - x^A_{\perp,j+1}) - 25/6\, x^A_4]\varepsilon_{AA}/kT + (x^A_{j-1} - x^A_{\perp,j-1}) + 4(x^A_j - \tfrac{1}{4}x^A_{//,j}) + 4(x^B_{j+1} - \tfrac{1}{4}x^B_{//,j+1}) + (x^B_{j+2} - x^A_{\perp,j+1})]\,\varepsilon_{AB}/kT = 0 \qquad (7)$$

and

$$\ln\{[2/4\, x_{//,j}(1-x_4)^2]/[(1-x_j)^2(x^A_4/6)]\} + [(x^A_{j-1} - x^A_{\perp,j-1}) + 3(x^A_j - \tfrac{1}{4}x^A_{//,j}) + (x^A_{j+1} - x^B_{\perp,j}) - 25/6\, x^A_4]\varepsilon_{AA}/kT + [(x^B_{j-1} - x^B_{\perp,j-1}) + 3(x^B_j - \tfrac{1}{4}x^B_{//,j}) + (x^B_{j+1} - x^A_{\perp,j}) - 25/6\, x^B_4]\varepsilon_{BB}/kT + [(x^A_{j-1} - x^A_{\perp,j-1}) + 3(x^A_j - \tfrac{1}{4}x^A_{//,j}) + (x^A_{j+1} - x^B_{\perp,j}) + (x^B_{j-1} - x^B_{\perp,j-1}) + 3(x^B_j - \tfrac{1}{4}x^B_{//,j}) + (x^B_{j+1} - x^A_{\perp,j}) - 25/6\, x_4]\varepsilon_{AB}/kT = 0 \qquad (8)$$

(8)

Figure 4 shows the results of segmental density calculations for the first layer at ε_{AA}/kT=*-0.6*, ε_{AB}/kT= *-0.1*, ε_{BB}/kT = *-0.2*, ε_{AS}/kT = *-1.0*, ε_{BS}/kT = *-0.3* and Monte Carlo simulation data. As seen from Figure 4, theoretical predictions are in excellent agreement with the simulations.

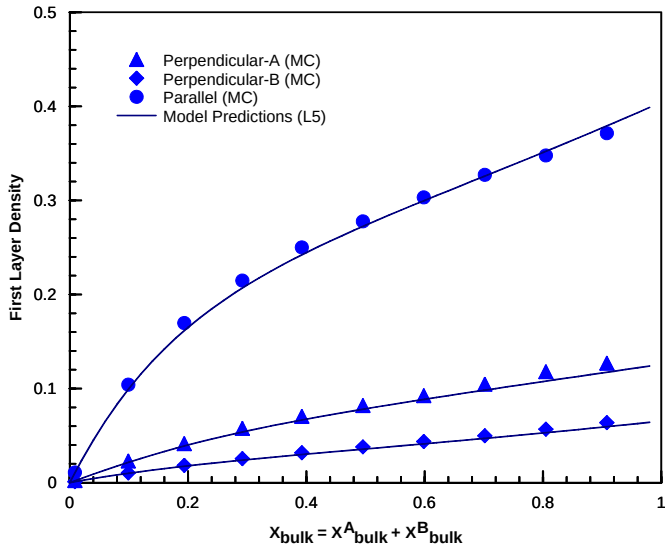

Figure 4. Amphiphilic dimer adsorption at surfaces. The energy parameters used here are: ε_{AA}/kT = *-0.6*, ε_{AB}/kT = *-0.1*, ε_{BB}/kT = *-0.2*, ε_{AS}/kT = *-1.0*, ε_{BS}/kT = *-0.3*.

This work is described in more detail in the paper "Adsorption of Amphiphilic Dimers at Surfaces" that appeared in *Journal of Colloid and Interface Science* **230,** 281 (2000).

Amphiphilic Dimers in Solution

In the previous section, we considered a lattice Density Functional Theory to study the adsorption behavior of dimers at flat surfaces. Although the interactions of dimers in solution can be conceptualized as the adsorption of dimers on a central dimer molecule, the actual behavior is more complicated because it is necessary to consider the three-dimensional arrangement of molecules [16]. There have been no analytic models capable of predicting the highly non-ideal behavior of asymmetric dimers in solution.
In a lattice system, an amphiphilic dimer has only one axis of symmetry. There are two ends (denoted as E) and eight sides (denoted as S) on the surface of a dimer as illustrated in Figure 6. The sites marked '1' are the sites adjacent to the dimer. The number '1' signifies that the site is within the first layer of segments adjacent to the central dimer. The '2' sites are located diagonally from the central segments. They are in the second shell from the central dimer. Sites marked with '3' are in the third shell, i.e. in the second layer from the dimer surface. Here, the 'B' sites are assumed to have bulk properties. The assumption that forth-nearest neighbors have bulk properties is valid for systems with low to moderate interaction energies. Also bear in mind that a site marked '2' in the

side view (the diagram on the right below) has only two neighbors in the first layer, and the other four neighbors all are assumed to have bulk densities. Those second layer sites in the side view are therefore marked as '2^S'. For the second layer in the end view (the diagram on the left below), there are two neighbors in the first layer, three neighbors in the bulk, and one neighbor in the same second layer. They are marked as '2^E', where the 'E' denotes the end view. There are eight '2^E' sites and eight '2^S' sites around a central dimer.

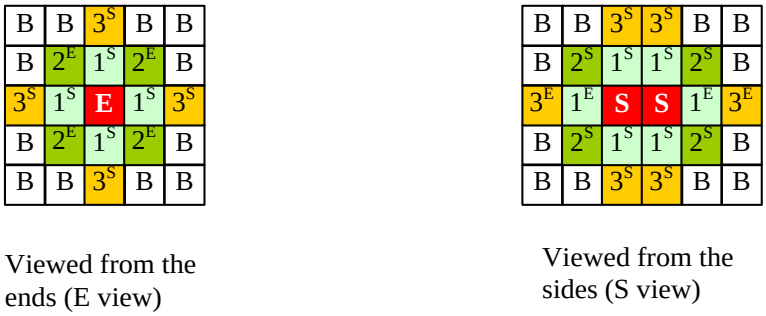

Figure 5. Shells around the central dimer.

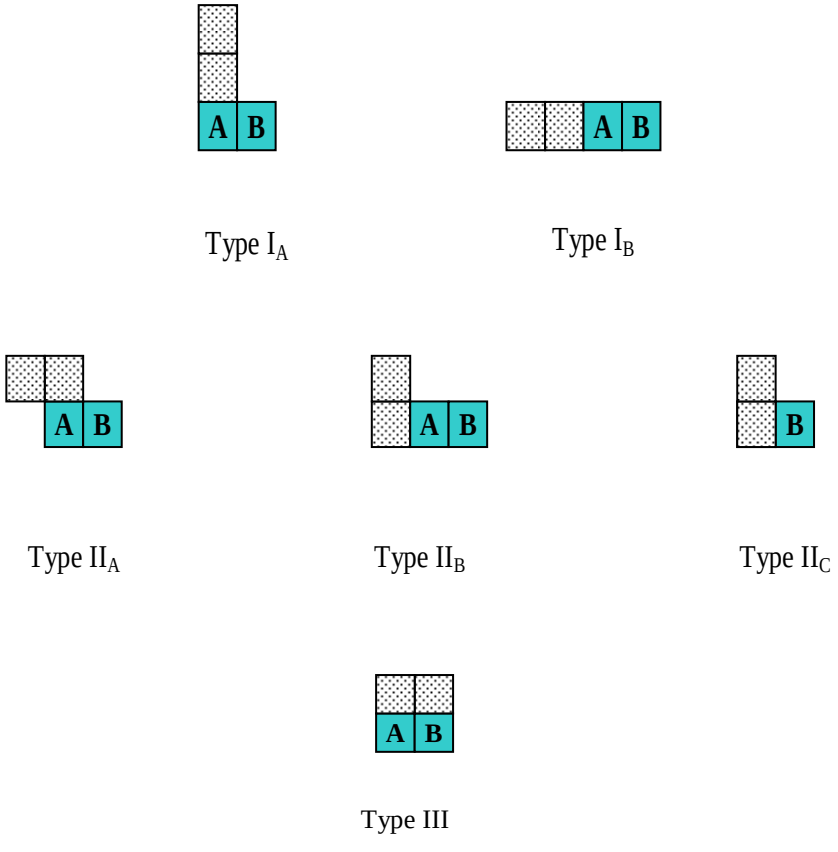

Figure 6. Dimer – dimer configurations.

There are three main 'types' of configurations for the surrounding dimers. The distinctions between these main types are the physical locations of the two occupied sites. Here, we consider only configurations illustrated in Figure 6 where the surrounding dimer can occupy sites in the first, second, or third shells around the central dimer. Figure 6 shows these configurations where the central dimer is marked AB.

Applying the DFT procedure for amphiphilic dimers results in the set of equations of equilibrium for probabilities of AA, AB, and BB bonds. In this section, we consider only two groups of configurations: in the first group, a neighboring dimer has only one bond with the central dimer; in the second group, there are two bonds with possible energies, ($\boldsymbol{g}_{AA} + \boldsymbol{g}_{BB}$) or $2\boldsymbol{g}_{AB}$. In the framework of this set of configurations, there are six variables: x_{AA} , x_{AB} , x_{BA} , x_{BB} , x_{ABAB} , and x_{ABBA} . Here subscript AA means that the A segment of the neighboring molecule has a link to the A segment of the central dimer, subscript AB means that the B segment of the neighboring molecule has a link to the A segment of the central dimer, etc. Subscript ABAB means that a neighboring dimer has both AA and BB links to the central dimer with energy ($\boldsymbol{g}_{AA} + \boldsymbol{g}_{BB}$). Subscript ABBA denotes that a neighboring dimer has two AB links to the central dimer with energy $2\boldsymbol{g}_{AB}$. Considering only these six configurations results in the following set of equations of equilibrium:

$$\ln\frac{x_{AB}(1-x_\infty)}{(1/3)x_\infty(1-x_{AA}-x_{AB}-x_{ABAB}-x_{ABBA})}+\frac{\varepsilon_{AB}}{kT}+\frac{\varepsilon_{BB}}{kT}(x_{BB}-x_\infty/2)+ \\ +\frac{\varepsilon_{AB}}{kT}(x_{BA}-x_\infty/2)-(\frac{\varepsilon_{BB}}{kT}+\frac{\varepsilon_{AB}}{kT})x_\infty/2=0 \tag{9}$$

$$\ln\frac{x_{BA}(1-x_\infty)}{(1/3)x_\infty(1-x_{BB}-x_{BA}-x_{ABAB}-x_{ABBA})}+\frac{\varepsilon_{AB}}{kT}+\frac{\varepsilon_{AA}}{kT}(x_{AA}-x_\infty/2)+ \\ +\frac{\varepsilon_{AB}}{kT}(x_{AB}-x_\infty/2)-(\frac{\varepsilon_{AA}}{kT}+\frac{\varepsilon_{AB}}{kT})x_\infty/2=0 \tag{10}$$

$$\ln\frac{x_{ABAB}(1-x_\infty)^2}{(1/12)x_\infty(1-x_{AA}-x_{AB}-x_{ABAB}-x_{ABBA})(1-x_{BB}-x_{BA}-x_{ABAB}-x_{ABBA})}+ \\ +\frac{\varepsilon_{AA}}{kT}+\frac{\varepsilon_{BB}}{kT}-(\frac{\varepsilon_{AA}}{2kT}+\frac{\varepsilon_{AB}}{kT}+\frac{\varepsilon_{BB}}{2kT})x_\infty=0 \tag{11}$$

$$\ln\frac{x_{BB}(1-x_\infty)}{(1/3)x_\infty(1-x_{BB}-x_{BA}-x_{ABAB}-x_{ABBA})}+\frac{\varepsilon_{BB}}{kT}+\frac{\varepsilon_{BB}}{kT}(x_{AB}-x_\infty/2)+ \\ +\frac{\varepsilon_{AB}}{kT}(x_{AA}-x_\infty/2)-(\frac{\varepsilon_{BB}}{kT}+\frac{\varepsilon_{AB}}{kT})x_\infty/2=0 \tag{12}$$

$$\ln \frac{x_{ABBA}(1-x_\infty)^2}{(1/12)x_\infty(1-x_{AA}-x_{AB}-x_{ABAB}-x_{ABBA})(1-x_{BB}-x_{BA}-x_{ABAB}-x_{ABBA})} + \quad (13)$$

$$+2\frac{\varepsilon_{AB}}{kT}-(\frac{\varepsilon_{AA}}{2kT}+\frac{\varepsilon_{AB}}{kT}+\frac{\varepsilon_{BB}}{2kT})x_\infty = 0$$

$$\ln \frac{x_{AA}(1-x_\infty)}{(1/3)x_\infty(1-x_{AA}-x_{AB}-x_{ABAB}-x_{ABBA})}+\frac{\varepsilon_{AA}}{kT}+\frac{\varepsilon_{AA}}{kT}(x_{BA}-x_\infty/2)+$$

$$+\frac{\varepsilon_{AB}}{kT}(x_{BB}-x_\infty/2)-(\frac{\varepsilon_{AA}}{kT}+\frac{\varepsilon_{AB}}{kT})x_\infty/2=0 \quad (14)$$

Figure 7 shows the internal energy predicted by the lattice DFT and obtained from Monte Carlo simulations for $\varepsilon_{AA}/kT = -0.5$, $\varepsilon_{AB}/kT = +0.4$, and $\varepsilon_{BB}/kT = -0.3$. Also shown are predictions of the mean-field theory (dashed line). As seen from Figure 7, the developed model predictions are in agreement with Monte Carlo simulations, and mean-field predictions are significantly off the Monte Carlo results.

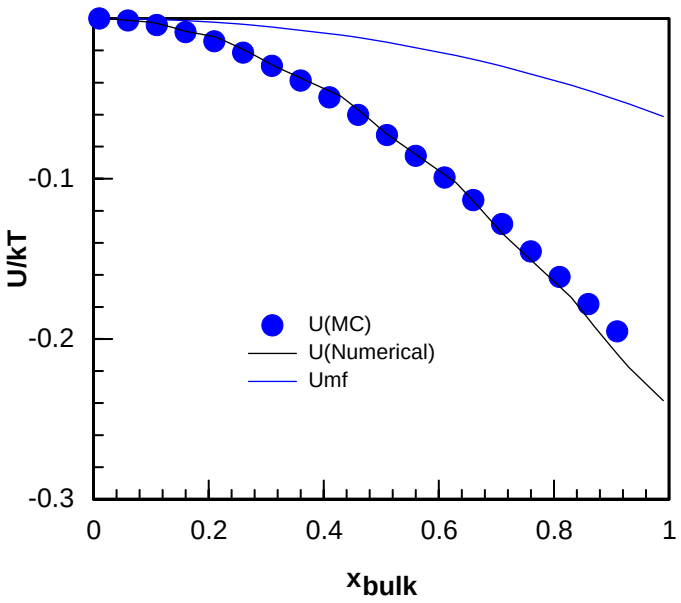

Figure 7. Dependence of internal energy, U, on x_4 at $\varepsilon_{AA}/kT = -0.5$, $\varepsilon_{AB}/kT = +0.4$, and $\varepsilon_{BB}/kT = -0.3$ **.**

This work is described in more detail in the paper "Nonrandom Behavior of Amphiphilic Dimers in Solution" that appeared in *Journal of Chemical Physics* **113**, 3404 (2000).

Lamellization and Micellization

We have observed a wide variety of phase behavior for asymmetric dimers, including formation of lamellae and micelles. Figure 8 illustrates the formation of lamella observed in canonical Monte Carlo simulations performed for amphiphilic dimers in a 20x20x20 box with periodic boundary conditions at $x_4 = 0.08$, $\varepsilon_{AA}/kT = \varepsilon_{BB}/kT = -1.5$, and $\varepsilon_{AB}/kT = +4$. The system was equilibrated for two million steps and then run for eight hundred million steps. As seen from Figure 8, the cluster has four sheets of AB molecules, and an ordered lamellar cluster coexists with a disordered vapor of amphiphilic dimers. The open segments on the right-hand side of the simulation box are the periodic boundary conditions for the cluster on the left.

A system with micelles is illustrated in Figure 9. These simulations were run for conditions where the three-dimensional phase transition is suppressed by repulsive forces between the head segments at $x_4 = 0.2$, $\varepsilon_{AA}/kT = -7$, $\varepsilon_{BB}/kT = \varepsilon_{AB}/kT = 4$. Though such parameters are physically unrealistic for non-ionic surfactants, they could be a reasonable assumption for ionic surfactants.

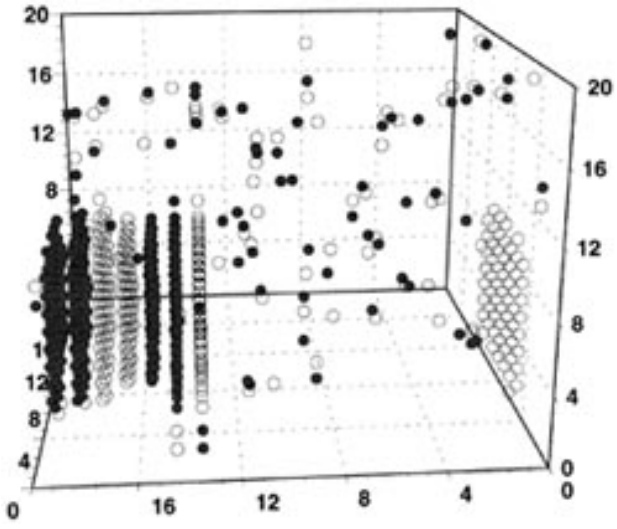

Figure 8. An ordered lamellar cluster of AB amphiphiles at $x_4 = 0.08$, $\varepsilon_{AA}/kT = \varepsilon_{BB}/kT = \varepsilon_{AA}/kT = -1.5$, and $\varepsilon_{AB}/kT = 4$.

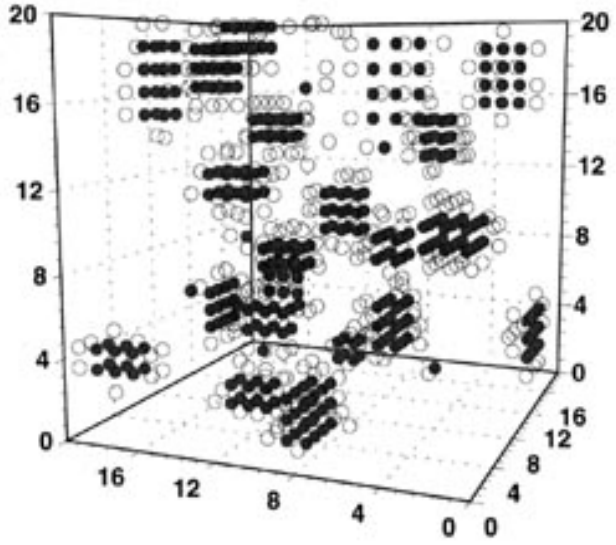

Figure 9. Amphiphilic dimers showing the formation of micelles at $x_4 = 0.2$, $\varepsilon_{AA}/kT = -7$, and $\varepsilon_{BB}/kT = \varepsilon_{AB}/kT = 4$.

Block Copolymers

Configurational Probabilities

Block copolymers are used widely in modern technology and science [17-19]. In particular, block copolymers exhibit a broad range of material properties due to the variety of sub-molecular structures that can form [20, 21]. These structures result from

preferential molecular configurations due to segmental interactions between copolymer chains [22, 23].

Here, phase transitions in block copolymers are considered in terms of configurational probabilities, p_n , and ordering transitions appear as a stepped increase in the probability of a dominating configuration and a simultaneous decrease of the probabilities for other configurations. To illustrate this, consider an exchange of a test AABBBBBAA molecule from n-th configuration and chain of nine vacancies in the bulk:

$$AABBBBBAA_n + VVVVVVVVV_b = AABBBBBAA_b + VVVVVVVVV_n \qquad (15)$$

where the subscript *n* denotes n-th configuration, subscript *b* denotes a bulk phase where there are random configurations of the molecules, and VVVVVVVVV is the vacancy chain. If this exchange occurs at equilibrium, then:

$$\Delta U - T\Delta S = 0 \qquad (16)$$

where ΔU and ΔS are the internal energy and entropy changes, and T is the absolute temperature. In the mean-field approximation, ΔS and ΔU can be represented in the following form:

$$\Delta S = k \ln \frac{p_n (1 - x_A - x_B)^{l_A + l_B}}{(1 - \sum_{n=1}^{N_c} p_n)^{l_A + l_B} (x_A + x_B)} \qquad (17)$$

$$\Delta U = -[E_n + (z_c - 1)\, p_n E_n - z_c l_A (\varepsilon_{AA} x_A + \varepsilon_{AB} x_B) - z_c l_B (\varepsilon_{AB} x_A + \varepsilon_{BB} x_B)] \qquad (18)$$

where x_A and x_B are segmental fractions of A and B components respectively, l_A and l_B are numbers of A and B segments in a molecule of the copolymer, ε_{AA} , ε_{AB} , and ε_{BB} are energies of segment - segment interactions, E_n is the energy of the molecule - molecule interaction in the n-th configuration, and z_c is the number of possible neighbors around a copolymer segment. In our calculations, we consider a cubic lattice with $z_c = 4$. Negative values of ε_{AA} , ε_{AB} , and ε_{BB} imply molecular attractions. Note that $x_A / l_A = x_B / l_B$.

Substituting equations (17) and (18) into equation (16) gives:

$$kT \ln \frac{p_n (1 - x_A - x_B)^{l_A + l_B}}{(1 - \sum_{n=1}^{N_c} p_n)^{l_A + l_B} (x_A + x_B)} + E_n + (z_c - 1) p_n E_n - z_c l_A (\varepsilon_{AA} x_A + \varepsilon_{AB} x_B) - z_c l_B (\varepsilon_{AB} x_A + \varepsilon_{BB} x_B) = 0 \qquad (19)$$

Figure 10 shows the probabilities, p_1 - p_5, for the various configurations as functions of x_A predicted by equation (19) at $\varepsilon_{AA}/kT = -0.36$, $\varepsilon_{AB}/kT = -0.09$, and $\varepsilon_{BB}/kT = 0$ and by Monte Carlo simulations.

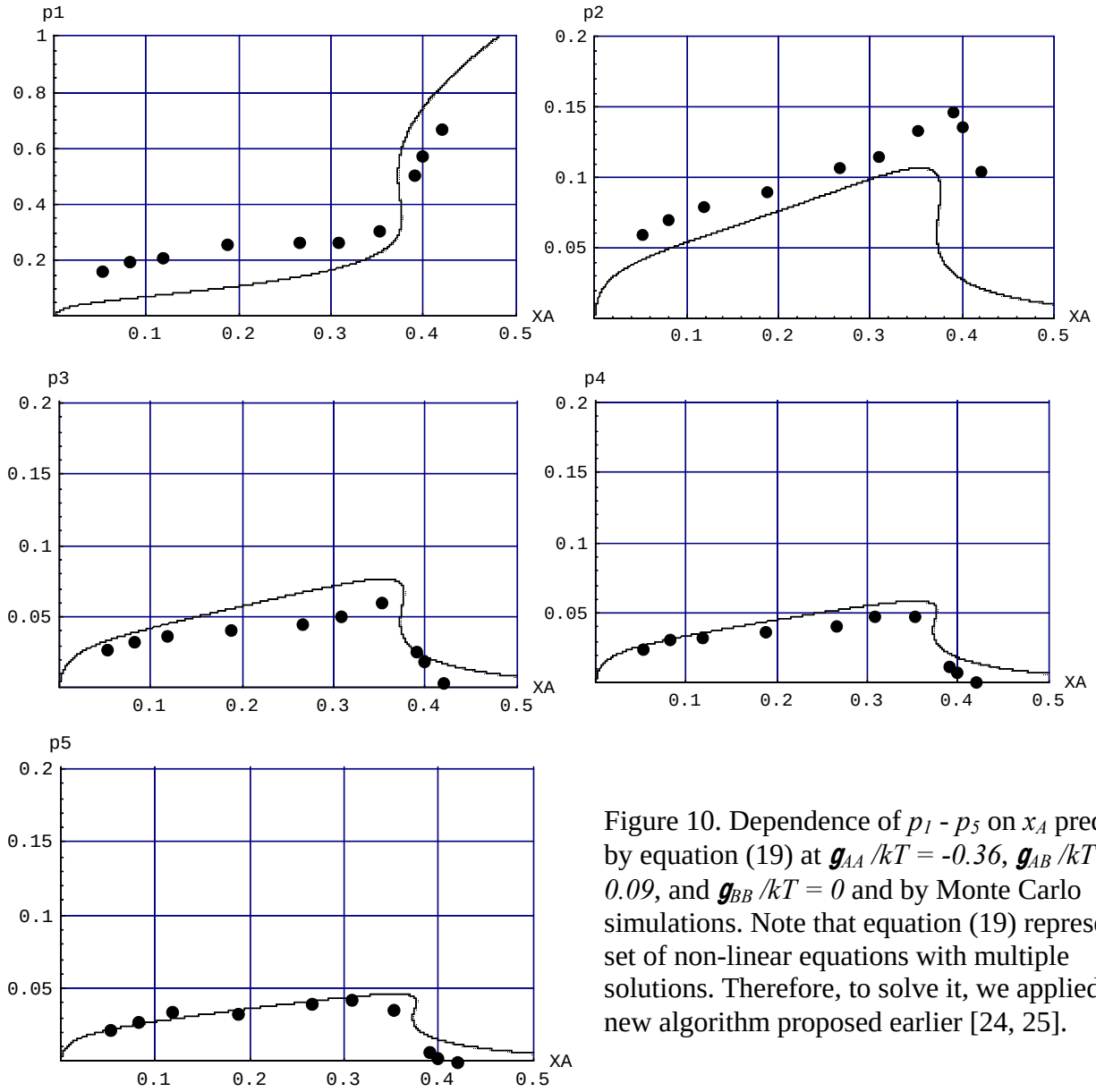

Figure 10. Dependence of p_1 - p_5 on x_A predicted by equation (19) at $\gamma_{AA}/kT = -0.36$, $\gamma_{AB}/kT = -0.09$, and $\gamma_{BB}/kT = 0$ and by Monte Carlo simulations. Note that equation (19) represents a set of non-linear equations with multiple solutions. Therefore, to solve it, we applied a new algorithm proposed earlier [24, 25].

As seen from Figure 10, there is a good qualitative agreement between theory and simulations. These results show that order - disorder phase transitions in block copolymers are accompanied by a dramatic increase of the probability of the dominant configuration and simultaneous decrease in the probabilities of all other configurations.

Random Mixing Entropy

Random mixing models provide a convenient and relatively simple means of predicting the thermodynamic equilibrium of randomly mixed systems. Additionally, it is convenient to model nonrandom mixed systems by predicting thermodynamic properties with the random mixing assumption to which corrections can be applied. As Flory, Huggins, Guggenheim, and others developed entropy of mixing models for polymer solutions and blends more than 50 years ago, similar approaches can be applied to develop entropy of mixing models for copolymer solutions, melts, and blends.

Recently, Martinez [26] has rederived Guggenheim's configurational entropy model. Following Martinez, the total number of distinguishable configurations, W of a lattice system can be specified in terms of the molecular geometric constant of a type i molecule, $_i$, the number of molecules of type i, n_i, the number of lattice sites occupied by a type i molecule, r_i, m types of distinguishable molecules, the number of interactions, I, the number of bonds of type j, B_j, and b types of bonds:

$$W = \left[\prod_{i=1}^{m}(\zeta_i)^{n_i}\right]\frac{\left(\sum_{i=1}^{m} r_i n_i\right)!}{\prod_{i=1}^{m}(r_i n_i)!}\frac{I!\prod_{j=1}^{b} B_j!}{\left(I+\sum_{j=1}^{b} B_j\right)!} \qquad (20)$$

Using this approach, a random-mixing expression for the change in free energy of a diblock copolymer microphase separation transition (Figure 11) has been derived:

$$\frac{\Delta S_{MST}}{k_B} = -n_P \ln\frac{(r_P-1)}{2(z-1)^2 r_P} - (r_P-2)n_P \ln\frac{r_P-1}{r_P-2} - \tfrac{1}{2}[(z\,r_P+2)n_P]\ln\frac{z\,r_P}{(z\,r_P+2)}$$

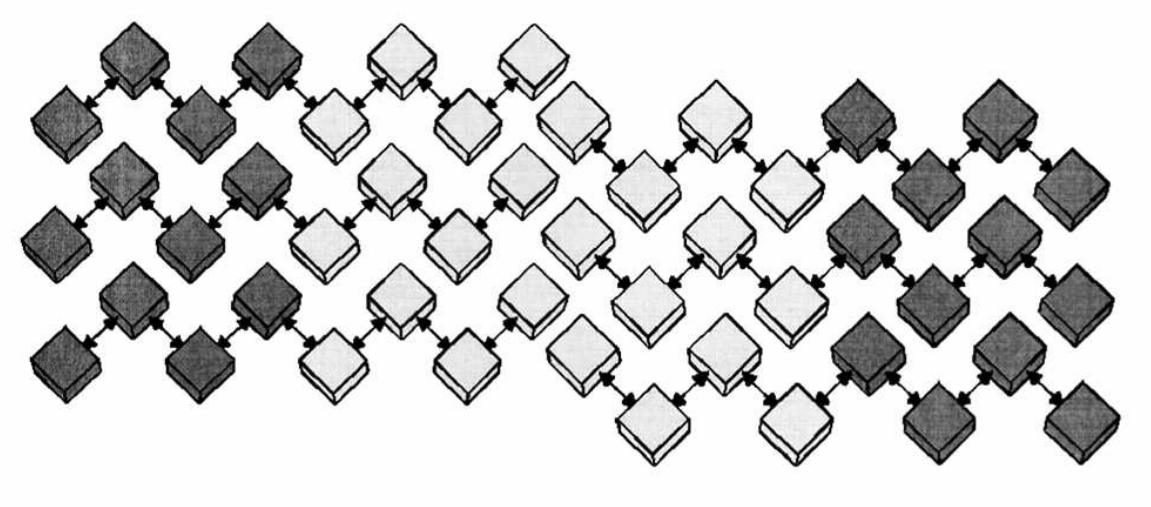

Figure 11. Illustration of microphase separation transition of diblock copolymers.

The ratio of phase transition temperatures of the demixing of a homopolymer blend and the microphase separation of a diblock copolymer with blocks of equal length is close to the result of Leibler's [27] mean field prediction for long chains as can be seen in Figure 12. Unlike Leibler's approach which is not accurate for short copolymer chains, this approach provides results including the dimer limit.

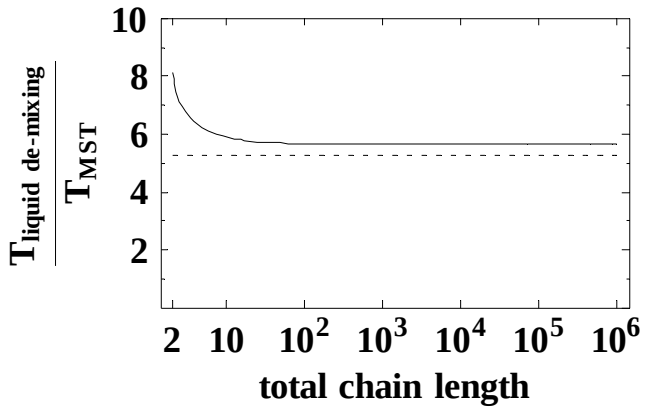

Figure 12. The ratio of the liquid de-mixing temperature of an equimolar homopolymer A and homopolymer B blend with no vacancies over the microphase separation transition temperature of a symmetric AB diblock copolymer melt with no vacancies is predicted as a function of the total chain length. Leibler's mean-field prediction (dashed) of this ratio is also shown.

Systems with Order - Disorder Transitions

Ordering is one of the most important phenomena in understanding phase transitions in co-polymers and co-polymer mixtures. That is why, the next step of our research was a study of the mechanism of ordering in the model with both attractive and repulsive interactions.

Order-disorder phase transitions have been studied extensively [28-33] by various methods including cell theory [34-38], density functional theory [39-42], and Monte Carlo simulations [43].

Special approaches have been developed for the analysis of disordered fluid to crystal transitions in the framework of lattice gas models. Although the early versions of the lattice gas model (Ising model) have been used for analysis of gas-liquid equilibrium [44], considerable effort has been directed to the phenomena of crystallization [45] by considering excluded shells. In these models, occupancy in the first shell, second shell, and, in some cases, even more distant shells is forbidden. Different types of potential functions also have been considered, including hard spheres [46], square well potentials [47], and repulsions with large positive (but not infinite) energies [48, 49]. It has been shown that models with first-neighbor exclusions give second-order phase transitions [50], but models with larger exclusion shells can give a first-order transition [51-53].

In this research, we derive the free energy as a density functional and then use the method of Lagrange's multipliers to minimize the grand potential. The result of this procedure is a finite-difference equation with respect to the density distribution, $\rho_{i,j,k}$. Consider a lattice gas (fluid) where i, j, and k are the three dimensions of the lattice coordinates. Each site of the lattice either is occupied by a molecule or is empty. There are repulsive interactions between nearest neighbors with being the energy of this repulsion (> 0). One molecule is considered as a central molecule with coordinates 0, 0, 0. To describe correlations between the central and surrounding molecules we consider correlations of other molecules around this central molecule.

Here, we consider repulsions between molecule at (i, j, k) and molecule at (i_1, j_1, k_1) where i_1 can be $i\pm1$ or i, j_1 can be $j\pm1$ or j, and k_1 can be $k\pm1$ or k. This is equivalent to prior work which considered repulsions for the first three nearest neighbors (shells) around a central molecule [40]. We also consider attractions between molecule at (i, j, k) and molecule at (i_2, j_2, k_2) where i_2 can be $i\pm2$, $i\pm1$ or i, j_1 can be $j\pm2$, $j\pm1$ or j, and k_1 can be

$k\pm2$, $k\pm1$ or k, assuming attractions between the central molecule and the fourth and fifth shells. With these pair interactions, Hamiltonian, H, can be written in the following form:

$$H=(\tfrac{1}{2})\sum_{i=-i^*}^{i^*}\sum_{j=-j^*}^{j^*}\sum_{k=-k^*}^{k^*}\rho_{i,j,k}\,[\varepsilon_1(R_1+R_2+R_3)+\varepsilon_2(R_4+R_5)] \qquad (21)$$

with

$$R_m=\sum_{(i',j',k')\subset S_m}\rho_{i',j',k'} \qquad (22)$$

where summation goes over all (i',j',k') from the sets of sites, S_m , defined as follows:
$\mathcal{C}S_1$ is the set of sites $(i\pm1, j, k)$, $(i, j\pm1, k)$, and $(i, j, k\pm1)$;
$\mathcal{C}S_2$ is the set of sites $(i\pm1, j\pm1, k)$, $(i, j\pm1, k\pm1)$, and $(i\pm1, j, k\pm1)$;
$\mathcal{C}S_3$ is the set of sites $(i\pm1, j\pm1, k\pm1)$;
$\mathcal{C}S_4$ is the set of sites $(i\pm2, j, k)$, $(i, j\pm2, k)$, and $(i, j, k\pm2)$;
$\mathcal{C}S_5$ is the set of sites $(i\pm2,j\pm1,k)$,$(i\pm2,j,k\pm1)$,$(i,j\pm2,k\pm1)$,$(i\pm1,j\pm2,k)$,$(i,j\pm1,k\pm2)$,$(i\pm1,j,k\pm2)$.

In equation (21), ε_1 is the energy of repulsion (>0) and ε_2 is the energy of attraction (<0). Equation (21) remains valid if we stipulate that $\rho_{0,0,0}=1$. Equation (21) for Hamiltonian gives the following equation of equilibrium:

$$\ln\{[\rho_{i,j,k}(1-\rho_\infty)]/[(1-\rho_{i,j,k})\rho_\infty]\}+[\varepsilon_1(R_1+R_2+R_3-26\rho_\infty)+\varepsilon_2(R_4+R_5-30\rho_\infty)]/k_BT=0 \qquad (23)$$

Figures 13 and 14 illustrate the changes in the density distribution around the central molecule in the vicinity of the order-disorder phase transition for $z=6$, $\rho_\infty=0.125$, $\varepsilon_2/k_BT=0$, and various ε_1/k_BT . As shown in Figure 13, at $\varepsilon_1/k_BT=0.9$, there are oscillations of the density around the central molecule, but the amplitude of these oscillations decays rapidly. Figure 14 shows that, at $\varepsilon_1/k_BT=0.93$, the character of the density distribution dramatically changes: there still are oscillations around the central molecule, but their amplitude does not decay and remains finite even far away from the central molecule. The order-disorder phase transition occurs at ε_1/k_BT between 0.9 and 0.93.

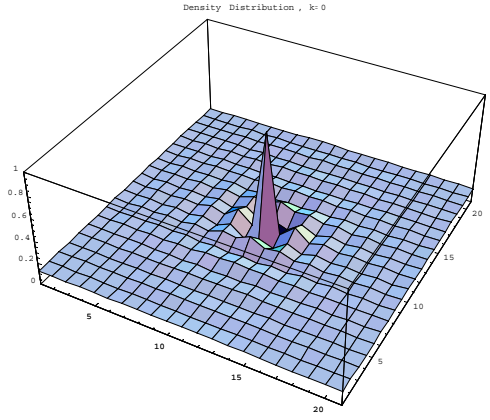

Figure 13. Density distribution around central molecule in the plane with $k=0$ for $\rho_4=0.125$, $\varepsilon_2/k_BT=0$, and $\varepsilon_1/k_BT=0.9$.

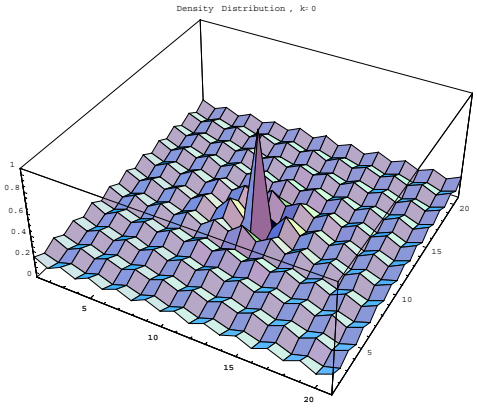

Figure 14. Density distribution around central molecule in the plane with $k=0$ for $\rho_4=0.125$, $\varepsilon_2/k_BT=0$, and $\varepsilon_1/k_BT=0.93$.

This work is described further in the paper “Lattice density functional theory predictions of order-disorder phase transitions” that has been published in *Journal of Chemical Physics* **115**, 2361-2366 (2000).

Self-Assembly

The potential for making self-assembled structures provides numerous opportunities for new technologies in nano-electronics [54], nonlinear optics [55], block copolymers [56] and conducting polymers [57], radiation absorbing materials [58], materials for artificial muscles [59], nano-materials [60, 61], supramolecular structures on surfaces [62], as well as lamellar and micellar systems [63]. The common feature of all self-assembled systems is that they have complex geometric structures with local order. The ability to form these complex structures depends on the geometry of molecules and on their intermolecular interactions.

Self-assembly has been defined as "the process by which a complex macromolecule (as collagen) or a supramolecular system (as a virus) spontaneously assembles itself from its components" [64]. In this research, the fundamentals of equilibrium self-assembly have been studied to learn how supramolecular structures can form by phase transitions in fluids. A lattice density functional theory (LDFT) is developed to describe this equilibrium self-assembly.

In the mean field approximation, the energy of interaction, E, between molecules sitting on two neighboring sites is

$$E = (1/2) \sum\sum \varepsilon_{mn} p(m) p(n) \tag{24}$$

where $p(m)$ and $p(n)$ are independent probabilities of having molecules on the sites with orientations providing contact of m-th and n-th contact points, ε_{mn} is the energy of interaction between m-th and n-th contact points, and the summation goes over all possible orientations.

Here, a complex fluid is modeled by asymmetric segments with directional interactions. It is shown that it is the directional interactions that allow processes akin to self-assembly. To illustrate this, consider a two-dimensional system on a square lattice. Each site (i, j) of this lattice either can be occupied by one molecule or empty and each molecule can have one of four different orientations. Applying LDFT for this system gives:

$$x_{k,i,j} = \frac{x_\infty \exp(-E_k)}{4(1-x_\infty) + x_\infty \sum_{k=1}^{4} \exp(-E_k)} \tag{25}$$

where $x_{1,i,j}$, $x_{2,i,j}$, $x_{3,i,j}$, and $x_{4,i,j}$ are order parameters, i.e. the probabilities of finding a molecule of each orientation at each site, and E_k is the energy of the segment in k-th orientation.

Figure 15 shows densities at each position, $x_{1,i,j} + x_{2,i,j} + x_{3,i,j} + x_{4,i,j}$, as a function of i and j at $T = 130$ K, $\varepsilon_{11} = -200$ K, $\varepsilon_{22} = -1000$ K, and all other ε_{mn} being zeros. As seen from Figure 15, decreasing temperature from 130 K to 127.94 K results in self-assembly of stepped lamellae from dimers. In general, the matrix $\|\varepsilon_{mn}\|$ is a primordial code for the structure of the fluid and for self-assembly of nano-scale and supramolecular objects. This code determines possible spontaneous phase transitions in the system.

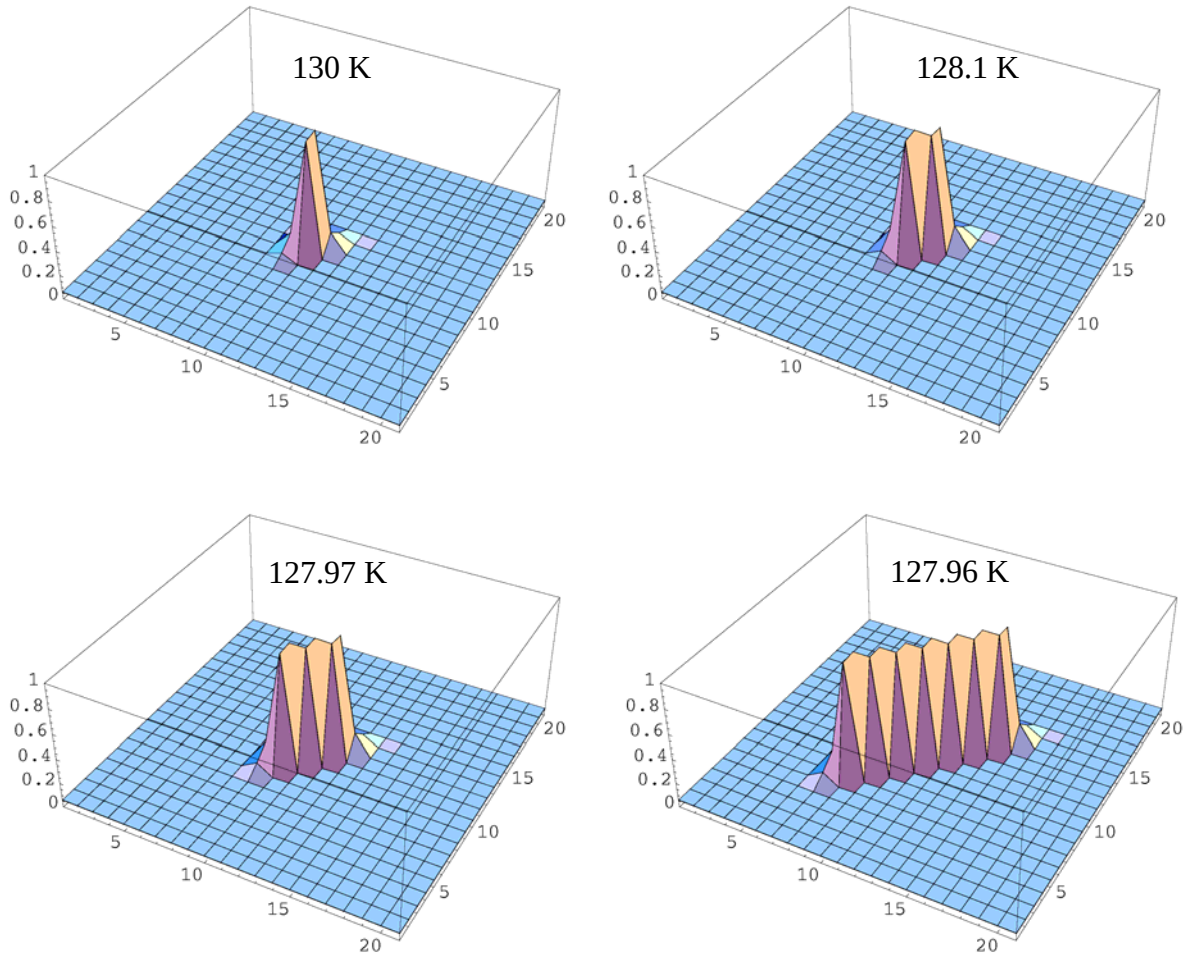

Figure 15. Self-assembly of stepped lamellae from dimers.

Phase Transitions in Systems with Directional Interactions

Density functional theories can result in accurate predictions of the free energy and phase transitions of a system. Applying the simplifications of only considering nearest neighbor interactions, and restricting the possible locations of components to a lattice can result in relatively simple expressions for the free energy.

With a simplification and generalization of a lattice density functional theory developed by Aranovich and Donohue [65], the free energy of a mixture including molecules with directional interactions has been derived:

$$\frac{A_{\text{mixture}}}{Nk_BT} = \sum_{i=1}^{\nu} x_i^{\infty} \ln x_i^{\infty} + \sum_{i=1}^{\nu}\sum_{m=1}^{\eta_i}\sum_{j=1}^{\nu}\sum_{n=1}^{\eta_j} \frac{x_i^{\infty} x_j^{\infty} \varepsilon_{[i,m][j,n]}}{2\eta_i k_B T} - \frac{1}{2}\sum_{i=1}^{\nu}\sum_{m=1}^{\eta_i} x_i^{\infty} \ln\left(\sum_{j=1}^{\nu}\sum_{n=1}^{\eta_j} \tau_{[j,n]}^{[i,m]}\right) \qquad (26)$$

where N is the number of lattice sites, k_B is Boltzmann's constant, T is the system temperature, ν is the number of types of components (including vacancies), x_i[4] is the probability of a random site containing a type i component, $\varepsilon_{[i,m][j,n]}$ is the interaction energy of the m^{th} side of type i component with the nth side of a type j component, η_j is the number of sides on a type i component, and

$$\tau_{[j,n]}^{[i,m]} = \frac{x_j^{\infty}}{\eta_j} \exp\left[\sum_{\ell=1}^{\nu} \sum_{p=1}^{\eta_\ell} \frac{x_\ell^{\infty} \left(\varepsilon_{[\ell,p][j,n]} - \varepsilon_{[i,m][j,n]} \right)}{\eta_\ell k_B T} \right] \tag{27}$$

The first two terms reduce to the Regular Solution Theory [66] when the molecules are homogeneous, the pure limits of the free energy of the mixture are subtracted from the free energy of the mixture to obtain the free energy of mixing, and the interaction energy between two molecules is approximated as the geometric mean of the respective pure-component interaction energies. The third term represents a nonrandom mixing correction to the random mixing free energy of the mixture.

As this free energy expression does not require every type of monomer to have the same number of sides, the phase behavior of mixtures molecules with different numbers of interaction sites can be predicted. For example, as can be seen in Fig. 16a, a binary mixture of 4-sided and 8-sided homogeneous monomers has two spinodal loops. Furthermore, as can be seen in Figs. 16b, 16c, and 16d, a binary mixture of 4-sided monomers with directional interactions and 8-sided homogeneous monomers, can have unusually shaped spinodal curves.

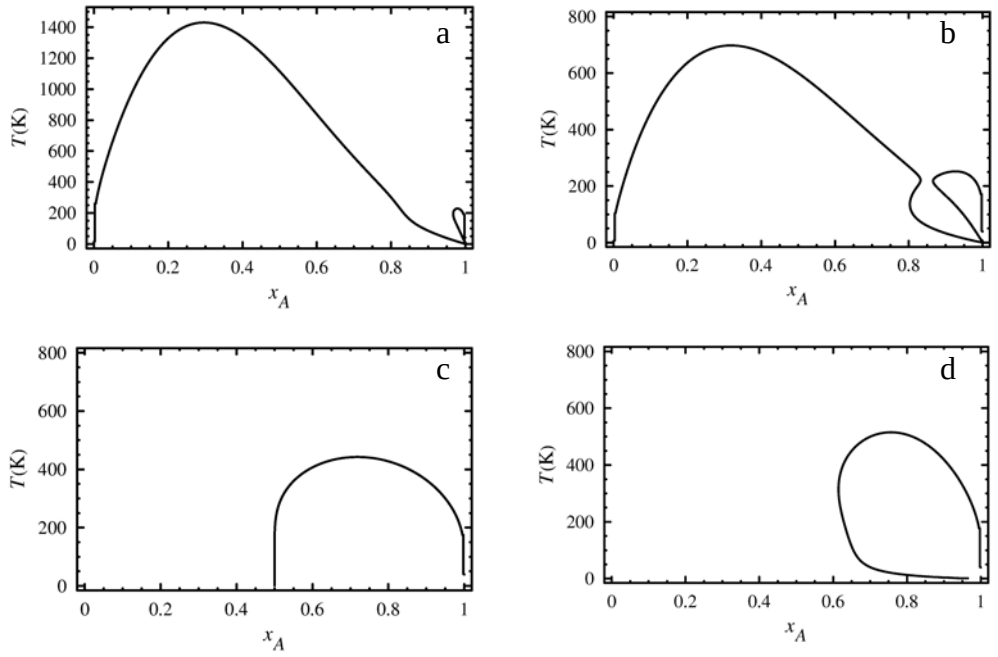

Figure 16a. A spinodal curve is presented for a binary mixture of homogeneous monomers of types A and B with no vacancies as a function of the mole fraction of A. Each type A monomer has 8 type α sides and each type B monomer has 4 type β sides where $\varepsilon_{\alpha\alpha} = \varepsilon_{\alpha\beta} = k_B$(-200 K) and $\varepsilon_{\beta\beta} = k_B$(-1100 K).

Figure 16b. A spinodal curve is presented for a binary mixture of type *A* homogeneous monomers and of type *B* monomers with directional interactions with no vacancies as a function of the mole fraction of *A*. Each type *A* monomer has 8 type α sides and each type *B* monomer has 2 type $\beta 1$ sides and 2 type $\beta 2$ sides where $\varepsilon_{\alpha\alpha} = \varepsilon_{\alpha\beta 1} = \varepsilon_{\alpha\beta 2} = k_B$ (-200 K), $\varepsilon_{\beta 1\beta 2} = k_B$ (-1100 K), and $\varepsilon_{\beta 1\beta 1} = \varepsilon_{\beta 2\beta 2} = 0$.

Figure 16c. A spinodal curve is presented for a binary mixture of type *A* homogeneous monomers and of type *B* monomers with directional interactions with no vacancies as a function of the mole fraction of *A*. Each type *A* monomer has 8 type α sides and each type *B* monomer has 2 type $\beta 1$ sides and 2 type $\beta 2$ sides where $\varepsilon_{\alpha\alpha} = \varepsilon_{\alpha\beta 1} = \varepsilon_{\alpha\beta 2} = k_B$ (-200 K), $\varepsilon_{\beta 1\beta 2} = k_B$ (-1100 K), and $\varepsilon_{\beta 1\beta 1} = \varepsilon_{\beta 2\beta 2} = k_B$ (700 K).

Figure 16d. A spinodal curve is presented for a binary mixture of type *A* homogeneous monomers and of type *B* monomers with directional interactions with no vacancies as a function of the mole fraction of *A*. Each type *A* monomer has 8 type α sides and each type *B* monomer has 2 type $\beta 1$ sides and 2 type $\beta 2$ sides where $\varepsilon_{\alpha\alpha} = \varepsilon_{\alpha\beta 1} = \varepsilon_{\alpha\beta 2} = k_B$ (-200 K), $\varepsilon_{\beta 1\beta 2} = k_B$ (-1100 K), and $\varepsilon_{\beta 1\beta 1} = \varepsilon_{\beta 2\beta 2} = k_B$ (1100 K).

Self-Assembly in Confined Fluids

Self-assembly is the spontaneous formation of complex, hierarchical structures from solutions of randomly oriented molecules. Molecular assemblies created in such a way are of great interest in materials science, as they represent a way to build complex structures from a "bottom-up" approach, as contrasted to the more typical "top-down" methodologies such as photolithography and the chemical vapor deposition technique. Because these structures sometimes mimic those found in living cells, the process of self-assembly is also of fundamental importance in the fields of biology and biotechnology. The goal of this work is to understand the phenomena of self-assembly using mathematically simple models.

In this work, a two-dimensional system consisting of monomers with directional interactions between two walls was modeled using lattice density functional theory (DFT) [14], with the goal of studying the phase behavior of the system. The molecules were modeled as having two different sides, denoted as A and B. Nearest neighbor molecule-molecule and molecule-wall interactions were explicitly accounted for in the model.

Four different types of behavior were observed in this study. First, the system was studied under low interaction potentials. This regime is important because it allows for detailed comparisons to commonly made approximations in experimental studies. In this work we specifically consider the Langmuir and Frumkin approximations. It also allows the results of the DFT model to be compared to Monte Carlo machine simulation data, which is a good test of the ability of the theory to capture the essential physics of the system. The second type of behavior studied was condensation transitions, which were found to occur when the three molecule-molecule interactions (A-A, B-B, and A-B) were equal and larger than –1.0 kT. Next, the ordering behavior of the system was examined, which was found to occur when one of the molecule-molecule interactions (here the A-A interaction) was significantly larger than the other two. Finally, complex

transitions in which all interactions were large were studied, which appeared to be a superposition of both ordering and condensation transitions.

In the low interaction limit, it was found that when molecule-molecule interactions were present in the system, there were significant deviations between the DFT predictions and the Langmuir and Frumkin approximations of the theory at moderate to high bulk concentrations of monomers. However, the DFT model predictions were closest to the machine simulation data. Of interest was the magnitude of the error in using the Frumkin approximation, which is commonly thought to be a good semi-theoretical model for real isotherm data. It was found that in cases where the final state of the system was ordered, the error in the Frumkin approximation was so large that even qualitative predictions of the system behavior were wrong.

The condensation transition was found to exist when the molecule-molecule interactions were relatively symmetric (almost equal to each other) and more attractive than –1.0 kT. Snapshots from Monte Carlo simulations in the two phase region showed that the condensed phase was liquid-like in the number of nearest neighbors, but unordered.

For systems in which one of the molecule-molecule interactions was significantly larger than the other two, ordering was observed. It was found that when the largest interaction was less attractive than –2.4 kT, the system became more ordered as the bulk concentration was increased. However, when this interaction was –2.4 kT or more attractive, the system ordered itself as a first-order phase transition (Figure 17). This transition is an order-disorder transition. It was found that the magnitude of the molecule-surface interactions could be used to control the orientation of the molecules in the ordered state. Monte Carlo simulations in the two phase region showed that the order-disorder transition resulted in the formation of long chains of molecules in the system (Figure 18); the orientation of these chains can be controlled by adjusting the molecule-surface interaction. There is some experimental evidence for the formation of these types of chain-like structures in real systems; one example is magnetorheological fluids which are exposed to a magnetic field.

Finally, by increasing all of the interactions in the system to large values, transitions can be observed which are a combination of both ordering and condensation. Similar to the order-disorder transitions, the molecule-surface interaction can be used to control the orientation of the ordered state. Monte Carlo simulation shows that the phase transition results in a condensed, liquid-like state, except that the final state is made of monomers which are all in the same orientation.

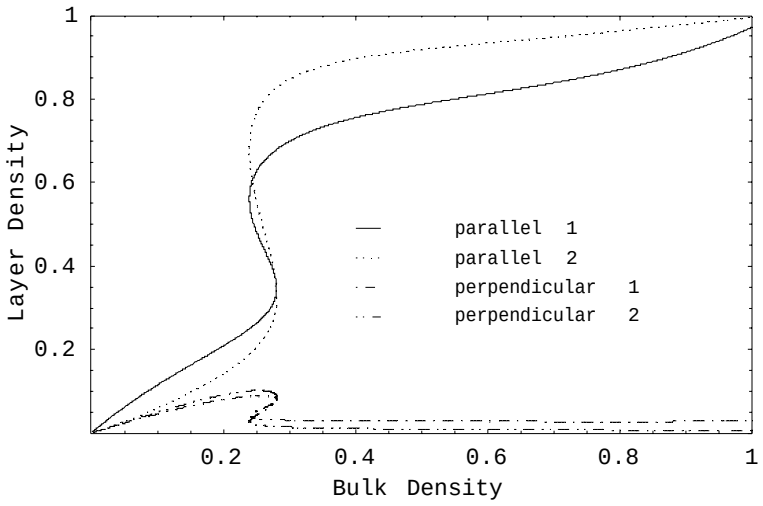

Figure 17. An order-disorder transition in a system with four layers between the two walls. Since the system is symmetric, only the results for the first two layers are presented. The two possible orientations of the molecules are denoted as parallel and perpendicular. The predictions are from the DFT model.

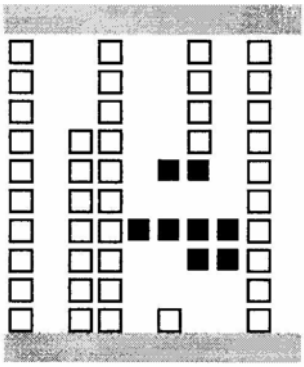

Figure 18. A Monte Carlo snapshot of a system with ten layers after an order disorder transition. The formation of chain-like structures is apparent. In the figure, the open squares represent monomers in the parallel orientation, while the filled squares are monomers in the perpendicular orientation.

Critical Point Corrections

Studying crossover between mean-field behavior and critical behavior [67] provides important insights into the thermodynamics of fluids and liquid mixtures over the entire range of conditions [68]. However, rigorous approaches are limited, and cannot be applied without further development to complex systems including self-assembled layers [69], colloid systems [70], and nano-phases [71, 72] where objects of different scales (nano-, meso-, and macro-) and different dimensionalities are in equilibrium.

For complex systems, mean-field approaches turn out to be useful [73-75], but the description of the system behavior close to the critical point has to be corrected. In this paper, we propose a simple method of correcting critical points for mean-field theory of adsorption. For this purpose, we consider Ono-Kondo lattice density functional theory [76, 77] which describes density gradients near phase boundaries and in nano-scale pores [78-81]. In the classical Ono-Kondo model [76], the vapor-liquid interface is represented by a lattice where each site either can be occupied by a molecule or empty. Ono-Kondo theory also has been applied to liquid-solid and gas-solid interfaces [78-83].

Classical Ono-Kondo Theory

Consider a one-component lattice gas in contact with a surface (hard wall). There are interactions between nearest neighbors with ε being the energy of adsorbate - adsorbate interactions and ε_S being the interaction energy for adsorbate molecules at the adsorbent surface. (Both ε and ε_S are negative for attractive forces.) For one layer between two walls (Figure 19), the Ono-Kondo equation can be written in the following form:

$$\ln\frac{x_1(1-x_b)}{x_b(1-x_1)}+\frac{z_1\varepsilon_S}{kT}+\frac{z_2\varepsilon}{kT}x_1-\frac{z_3\varepsilon}{kT}x_b=0 \qquad (28)$$

In this equation, x_1 is the density or fraction of sites occupied by molecules in the adsorbed layer, x_b is the fraction of sites occupied with fluid molecules in the bulk, z_3 is the coordination number for three-dimensional lattice ($z_3 = 6$ for a cubic lattice), z_2 is the monolayer coordination number ($z_2 = 4$ for a square lattice), z_1 is the number of molecule-surface bonds ($z_1 = 2$ for one layer between two walls as shown in Figure 19), k is Boltzmann's constant, and T is the absolute temperature.

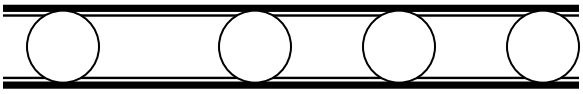

Figure 19. Cross section of the monolayer between two walls.

Equation (28) relates the density in the adsorbed layer with the density in the bulk. In earlier publications, we presented a numerical method of solving the Ono-Kondo equations when there are multiple solutions [84, 85]. A typical solution of equation (28) is illustrated in Figure 20 for $z_1 = 2$, $z_2 = 4$, $z_3 = 6$, $\varepsilon/kT = -1.3$ and $\varepsilon_S/kT = -1.0$. In Figure 20, points A and B indicate spinodals for two-dimensional condensation (in the

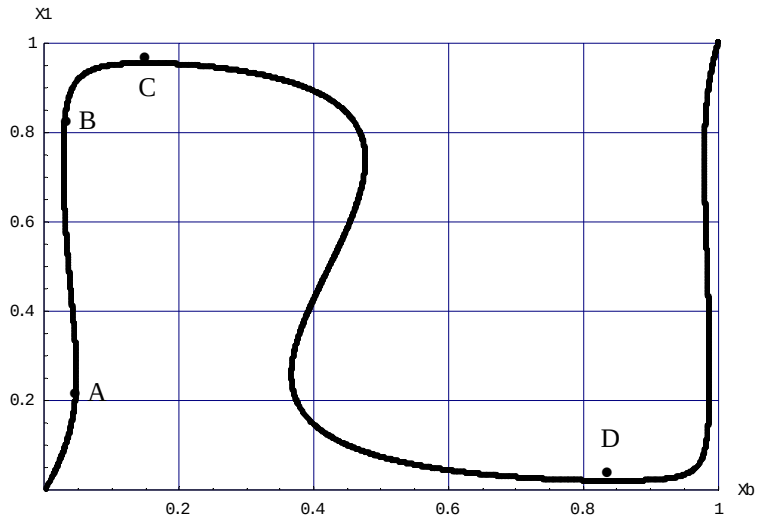

Figure 20. Typical solution for Ono-Kondo equation.

monolayer) and points C and D indicate spinodals for three-dimensional condensation (in the bulk). Hence, the Ono-Kondo equation not only gives the adsorption isotherm, but it also relates phase behavior in the adsorbed layer to the phase behavior in the bulk [81]. However, the Ono-Kondo model gives classical, mean-field phase diagrams and critical points [86-88]. In this paper, we propose a correction to the Ono-Kondo equation to describe phase behavior near the critical point more accurately.

Adsorption Equilibrium

Consider taking an adsorbate molecule from the adsorbed layer between two walls (Figure 19) and moving it to an empty site in the bulk. This is equivalent to the exchange of a molecule with a vacancy,

$$M_a + V_b \leftrightarrow V_a + M_b \qquad (29)$$

where M is the adsorbate molecule, and V is the vacancy (empty site) that it fills (and vice versa). If this exchange occurs at equilibrium, then:

$$\Delta U - T\Delta S = 0 \qquad (30)$$

where ΔU and ΔS are the enthalpy and entropy changes.

The value of ΔS can be represented in the form:

$$\Delta S = k_B \ln W_1 - k_B \ln W_2 \qquad (31)$$

where W_1 is the number of configurations where site in the adsorbed layer is occupied by an adsorbate molecule and the site in the bulk is empty, and W_2 is the number of configurations where the site in the bulk is occupied by an adsorbate molecule and site in the adsorbed layer is empty.

If the overall number of configurations for the system is W_0 , then:

$$W_1/W_0 = x_1 (1 - x_b) \qquad (32)$$

and

$$W_2/W_0 = x_b (1 - x_1) \qquad (33)$$

Substituting equations (32) and (33) into equation (31) we obtain

$$\Delta S = k \ln[x_1 (1 - x_b)/(1 - x_1)x_b] \qquad (34)$$

The change in enthalpy, ΔU, can be written as

$$\Delta U = E_a - E_b \qquad (35)$$

where E_a is the configurational energy of a molecule in the adsorbed layer, and E_b is the configurational energy of a molecule in the bulk. In the

classical (mean-field) approximation:

$$\frac{E_a}{kT} = -\frac{z_1 \varepsilon_S}{kT} - \frac{z_2 \varepsilon\, x_1}{kT} \tag{36}$$

and

$$\frac{E_b}{kT} = -\frac{z_3 \varepsilon\, x_b}{kT} \tag{37}$$

Substituting equations (36) and (37) into equation (35), and then equations (35) and (34) into equation (30) gives the classical Ono-Kondo equation (28) for a monolayer between two walls.

Equilibrium between Phases in the Bulk

Here, we assume molecules are in the two phase region for the three-dimensional lattice fluid. Consider taking a molecule from phase 1 and moving it to an empty site in phase 2. This is equivalent to the exchange of a molecule with a vacancy,

$$M_1 + V_2 \;\; 6 \;\; V_1 + M_2 \tag{38}$$

If this exchange occurs at equilibrium, then equation (30) also is valid, and it results in the following equation instead of equation (28):

$$\ln \frac{x_b^{'}(1-x_b^{''})}{x_b^{''}(1-x_b^{'})} + \frac{z_3 \varepsilon}{kT} x_b^{'} - \frac{z_3 \varepsilon}{kT} x_b^{''} = 0 \tag{39}$$

where $x_b^{'}$ and $x_b^{''}$ are the densities of phase 1 and phase 2.

Note that one-component lattice gas with nearest neighbors interactions is equivalent to classical Ising model [89] with symmetric phase diagram. Assuming that $x_b^{''} = 1 - x_b^{'}$, equation (39) can be written in the following form:

$$2 \ln \frac{x_b^{'}}{(1-x_b^{'})} + \frac{z_3 \varepsilon}{kT}(2x_b^{'} - 1) = 0 \tag{40}$$

which is the Bragg-Williams bimodal [89].

Spinodals

Differentiation of equation (28) with respect to x_b gives:

$$\frac{dx_1}{dx_b} = \frac{\dfrac{1}{x_b(1-x_b)} + \dfrac{z_3 \varepsilon}{kT}}{\dfrac{1}{x_1(1-x_1)} + \dfrac{z_2 \varepsilon}{kT}} \tag{41}$$

From equation (41), it follows that $dx_1/dx_b = 0$ if

$$\frac{1}{x_b(1-x_b)} + \frac{z_3 \varepsilon}{kT} = 0 \tag{42}$$

and $dx_1/dx_b = \infty$ if

$$\frac{1}{x_1(1-x_1)} + \frac{z_2\varepsilon}{kT} = 0 \qquad (43)$$

Note that equations (42) and (43) are the Bragg-Williams spinodals for the three-dimensional and two-dimensional lattices respectively [89]. Equation (41) can be written in a more general way:

$$\frac{dx_1}{dx_b} = \frac{f_3(x_b, T)}{f_2(x_1, T)} \qquad (44)$$

where equations

$$f_3(x_b,T)=0 \qquad (45)$$

and

$$f_2(x_1,T)=0 \qquad (46)$$

give the spinodals for three-dimensional and two-dimensional lattices respectively. Improving the functions $f_3(x_b,T)$ and $f_2(x_1,T)$ (compared to equation (41)) would allow more accurate predictions for equilibrium between adsorbed and bulk phases.

Improving Functions $f_3(x_b,T)$ and $f_2(x_1,T)$

Consider equations (36) and (37) as linear approximations for an expansion of the configurational energy in powers of density. Then, the series

$$\frac{E_a}{kT} = -\frac{z_1\varepsilon_S}{kT} - \frac{z_2\varepsilon\, x_1}{kT} + \alpha_a(T)x_1^2 + \beta_a(T)x_1^3 + \ldots \qquad (47)$$

and

$$\frac{E_b}{kT} = -\frac{z_3\varepsilon\, x_b}{kT} + \alpha_b(T)x_b^2 + \beta_b(T)x_b^3 + \ldots \qquad (48)$$

represent more exact expressions for E_a and E_b. Here α_a, β_a, α_b, and β_b are temperature dependent coefficients. Note that the quadratic and higher terms in equations (47) and (48) reflect correlations that become important near the critical point but which are not taken into account in the classical mean-field, Ono-Kondo model.

Using equations (47) and (48) instead of equations (36) and (37) and leaving only linear, quadratic, and cubic terms, we obtain instead of equation (41):

$$\frac{dx_1}{dx_b} = \frac{\dfrac{1}{x_b(1-x_b)} + \dfrac{z_3\varepsilon}{kT} - 2\alpha_b(T)x_b - 3\beta_b(T)x_b^2}{\dfrac{1}{x_1(1-x_1)} + \dfrac{z_2\varepsilon}{kT} - 2\alpha_a(T)x_1 - 3\beta_a(T)x_1^2} \qquad (49)$$

So:

$$f_3(x_b,T) = \frac{1}{x_b(1-x_b)} + \frac{z_3\varepsilon}{kT} - 2\alpha_b(T)x_b - 3\beta_b(T)x_b^2 \qquad (50)$$

and

$$f_2(x_1,T) = \frac{1}{x_1(1-x_1)} + \frac{z_2\varepsilon}{kT} - 2\alpha_a(T)x_1 - 3\beta_a(T)x_1^2 \qquad (51)$$

From statistical mechanics of the lattice gas [89], it is well known that both spinodals have to be symmetric. Hence

$$\beta_b(T) = -2\alpha_b(T)/3 \tag{52}$$

and

$$\beta_a(T) = -2\alpha_a(T)/3 \tag{53}$$

Therefore, the equations for spinodals are:

$$f_3(x_b, T) = \frac{1}{x_b(1-x_b)} + \frac{z_3\varepsilon}{kT} - 2\alpha_b(T)x_b(1-x_b) = 0 \tag{54}$$

and

$$f_2(x_1, T) = \frac{1}{x_1(1-x_1)} + \frac{z_2\varepsilon}{kT} - 2\alpha_a(T)x_1(1-x_1) = 0 \tag{55}$$

At the critical points, $x_1 = 0.5$ and $x_b = 0.5$. These requirements give from equations (54) and (55):

$$\alpha_a(T_2^{cr}) = 8 + 2\frac{z_2\varepsilon}{kT_2^{cr}} \tag{56}$$

$$\alpha_b(T_3^{cr}) = 8 + 2\frac{z_3\varepsilon}{kT_3^{cr}} \tag{57}$$

where T_3^{cr} and T_2^{cr} are critical temperatures for three- and two-dimensional lattices respectively.

In the vicinity of the critical point, there is a significant range of concentrations where the phase diagram is flat (and where T is almost constant). In this range,

$$\alpha_a(T) \approx \alpha_a(T_2^{cr}) \tag{58}$$

$$\alpha_b(T) \approx \alpha_b(T_3^{cr}) \tag{59}$$

Away from the critical point, the corrections $-2\alpha_b(T)x_b(1-x_b)$ and $-2\alpha_a(T)x_1(1-x_1)$ to the functions $f_3(x_b,T)$ and $f_2(x_1,T)$ vanish because factors $x_b(1-x_b)$ and $x_1(1-x_1)$ become small. Therefore, using approximations (58), (59) in equations (54) and (55) should be reasonable over a range of densities and temperatures. Plugging equations (56) and (57) into equations (54), (55), (58), (59) gives the following equations for spinodals (for two- and three-dimensional cases respectively):

$$-\frac{kT}{\varepsilon} = \frac{z_2}{\frac{1}{x_1(1-x_1)} - 4x_1(1-x_1)(4 + \frac{z_2\varepsilon}{kT_2^{cr}})} \tag{60}$$

$$-\frac{kT}{\varepsilon} = \frac{z_3}{\frac{1}{x_b(1-x_b)} - 4x_b(1-x_b)(4 + \frac{z_3\varepsilon}{kT_3^{cr}})} \tag{61}$$

Similarly, using the linear, quadratic, and cubic terms in equation (48) results in corresponding corrections to equation (39) and the following equation instead of equation (40):

$$2\ln\frac{x_b}{(1-x_b)}+z_3\frac{\varepsilon}{kT}(2x_b-1)+(8+2\frac{z_3\varepsilon}{kT_3^{cr}})[(1-x_b)^2-x_b^2+\frac{2}{3}x_b^3-\frac{2}{3}(1-x_b)^3]=0 \quad (62)$$

which gives the binodal for three-dimensional lattice:

$$-\frac{kT}{\varepsilon}=\frac{z_3(2x_b-1)}{2\ln\frac{x_b}{1-x_b}+(8+2\frac{z_3\varepsilon}{kT_3^{cr}})[1-2x_b+\frac{2}{3}x_b^3-\frac{2}{3}(1-x_b)^3]} \quad (63)$$

For two-dimensional case, equation (63) can be rewritten in the following form:

$$-\frac{kT}{\varepsilon}=\frac{z_2(2x_1-1)}{2\ln\frac{x_1}{1-x_1}+(8+2\frac{z_2\varepsilon}{kT_2^{cr}})[1-2x_1+\frac{2}{3}x_1^3-\frac{2}{3}(1-x_1)^3]} \quad (64)$$

Figures 21 and 22 show binodals predicted by equations (63) and (64) for two- and three-dimensional lattices, the exact 2D bimodal [89] and Monte Carlo simulation data for the 3D bimodal [90]. Also shown are binodals for quasichemical and Bragg-Williams approximations and spinodals predicted by equations (42), (43), (60), and (61).

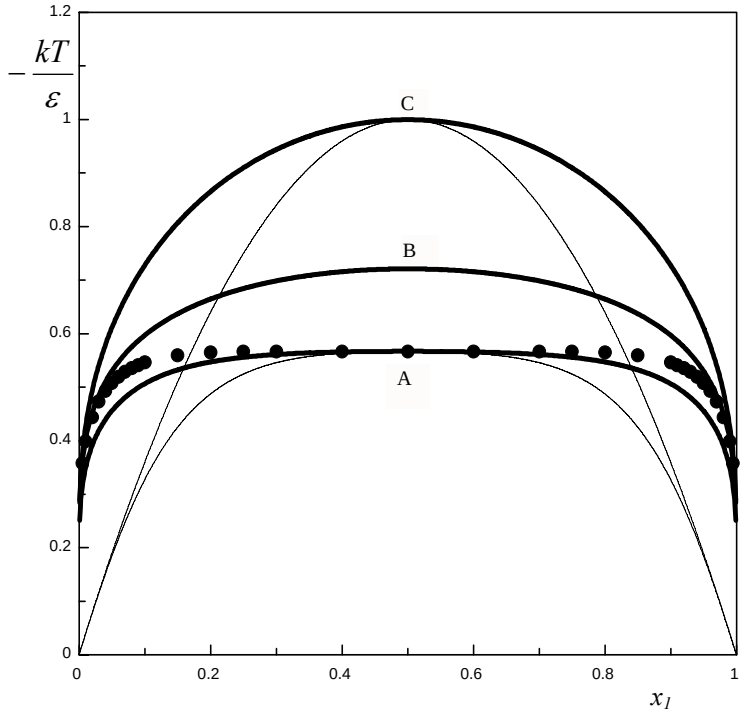

Figure 21. Binodals (thick lines) for two-dimensional lattice with $z_2 = 4$: A - predicted by equation (64); B - quasichemical; C - Bragg-Williams; solid circles show exact binodal from ref.[89]; thin lines show spinodals predicted by equations (43) and (60).

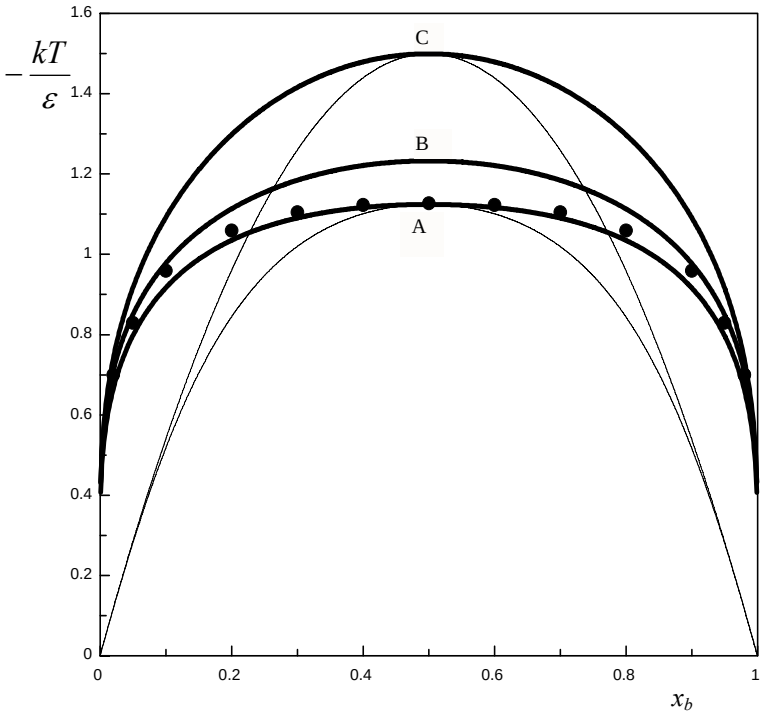

Figure 22. Binodals (thick lines) for three-dimensional lattice with $z_3 = 6$: A -predicted by equation (63); B - quasichemical; C - Bragg-Williams; solid circles show Monte Carlo simulation data for binodal from ref.[90]; thin lines show spinodals predicted by equations (42) and (61).

As shown by Figures 21 and 22, this new model predicts binodals which are in good agreement with exact results for 2D and with Monte Carlo simulation data for 3D. Though these results are quite good, there are errors at intermediate densities.

Scaling Behavior Near the Critical Point

Approximations (63) and (64) based on equations (58) and (59) give binodals which are exact at the critical point and in the limits of small and large densities. However, there are errors at intermediate densities (Figures 21 and 22). To reduce these errors, we consider a correction to equations (58) and (59) taking into account the temperature dependence of the coefficients α_a and α_b.

Consider expansion of $\alpha_a(T)$ and $\alpha_b(T)$ for subcritical temperatures in powers of t_a and t_b

$$t_a = \frac{T_2^{cr} - T}{T_2^{cr}} \qquad (65)$$

$$t_b = \frac{T_3^{cr} - T}{T_3^{cr}} \qquad (66)$$

in the form:

$$\alpha_a(T) = \mathrm{Re}(t_a) + Si(t_a) \tag{67}$$

$$\alpha_b(T) = \mathrm{Re}(t_b) + Si(t_b) \tag{68}$$

where *Re* and *Si* are regular and singular components defined as follows:

$$\mathrm{Re}(t_a) = \sum_{i=0}^{\infty} A_{ai} t_a^i \tag{69}$$

$$\mathrm{Re}(t_b) = \sum_{i=0}^{\infty} A_{bi} t_b^i \tag{70}$$

$$Si(t_a) = B_a t_a^{\nu_a} \tag{71}$$

$$Si(t_b) = B_b t_b^{\nu_b} \tag{72}$$

with $1 > \nu_a > 0$ and $1 > \nu_b > 0$.

Equations (67) – (72) give the following expansions for $\alpha_a(T)$ and $\alpha_b(T)$:

$$\alpha_a(T) = \alpha_a(T_2^{cr}) + B_a t_a^{\nu_a} + A_{a1} t_a + A_{a2} t_a^2 + \ldots \tag{73}$$

$$\alpha_b(T) = \alpha_b(T_3^{cr}) + B_b t_b^{\nu_b} + A_{b1} t_b + A_{b2} t_b^2 + \ldots \tag{74}$$

Equations (58) and (59) used only the first terms in the expansions (73) and (74). Now, we consider a second approximation - first two terms of the expansions - which gives:

$$\alpha_a(T) \approx \alpha_a(T_2^{cr}) + B_a t_a^{\nu_a} \tag{75}$$

$$\alpha_b(T) \approx \alpha_b(T_3^{cr}) + B_b t_b^{\nu_b} \tag{76}$$

With approximations (75) and (76) instead of (58) and (59), equations (63) and (64) can be rewritten in the following form:

$$-\frac{kT}{\varepsilon} = \frac{z_3(2x_b - 1)}{2\ln\frac{x_b}{1-x_b} + [8 + 2\frac{z_3\varepsilon}{kT_3^{cr}} + B_b(\frac{T_3^{cr} - T}{T_3^{cr}})^{\nu_b}][1 - 2x_b + \frac{2}{3}x_b^3 - \frac{2}{3}(1-x_b)^3]} \tag{77}$$

$$-\frac{kT}{\varepsilon} = \frac{z_2(2x_1 - 1)}{2\ln\frac{x_1}{1-x_1} + [8 + 2\frac{z_2\varepsilon}{kT_2^{cr}} + B_a(\frac{T_2^{cr} - T}{T_2^{cr}})^{\nu_a}][1 - 2x_1 + \frac{2}{3}x_1^3 - \frac{2}{3}(1-x_1)^3]} \tag{78}$$

In the limit of small t_a and t_b , equations (77) and (78) give:

$$\rho_a^L - \rho_a^G = const\ t_a^{\nu_a/2} \tag{79}$$

$$\rho_b^L - \rho_b^G = const\ t_b^{\nu_b/2} \tag{80}$$

where $\rho_a^L = 0.5 + \delta x_1$ (liquid density for 2D phase), $\rho_b^L = 0.5 + \delta x_b$ (liquid density for 3D phase), $\rho_a^G = 0.5 - \delta x_1$ (gas density for 2D phase), $\rho_b^G = 0.5 - \delta x_b$ (gas density for 3D phase), δx_1 and δx_b are variations of x_1 and x_b near the critical value (0.5). Equations (79) and (80) coincide with well-known equation for densities of coexisting phases near the critical point if $\nu_a /2$ and $\nu_b /2$ coincide with critical exponent β for two and three dimensions respectively [77]. Then:

$$\nu_a = 2\beta_a \tag{81}$$

$$\nu_b = 2\beta_b \tag{82}$$

Note that $\beta_a = 1/8$ and $\beta_b \approx 0.325$ for 2D and 3D Ising models respectively.

Figure 23 shows binodal for two-dimensional (square) lattice predicted by equation (78) at $B_a = 3.5$ and $\nu_a = ¼$. Also shown is exact bimodal [89] and binodal predicted by equation (64). As seen from Figure 23, using the appoximation (75) instead of (58) makes the error in predictions very small.

Figure 24 gives the binodal for the three-dimensional (cubic) lattice predicted by equation (77) with $B_b = 2$ and $\nu_b = 0.65$ compared to Monte Carlo simulation data. Also shown are predictions of equation (63). As seen from Figure 24, approximation (76) gives excellent agreement between theoretical binodal and Monte Carlo simulations.

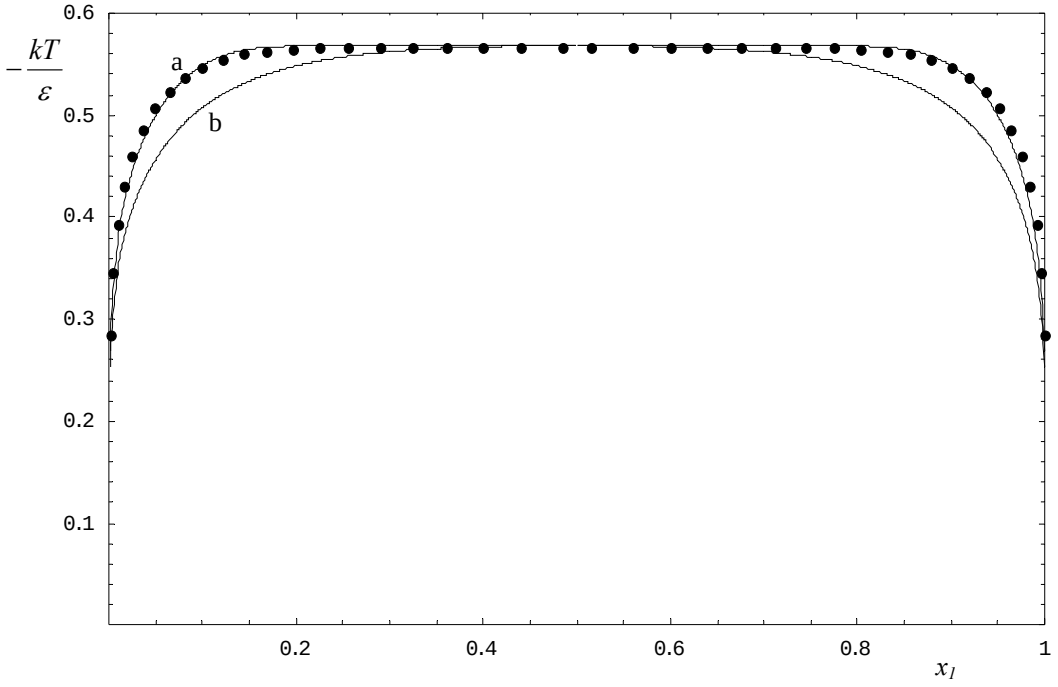

Figure 23. Binodal for two-dimensional (square) lattice: (a) - equation (78); (b) - equation (64); solid circles show exact binodal from ref.[89]. Here $B_a = 3.5$, and $\nu_a = 0.25$.

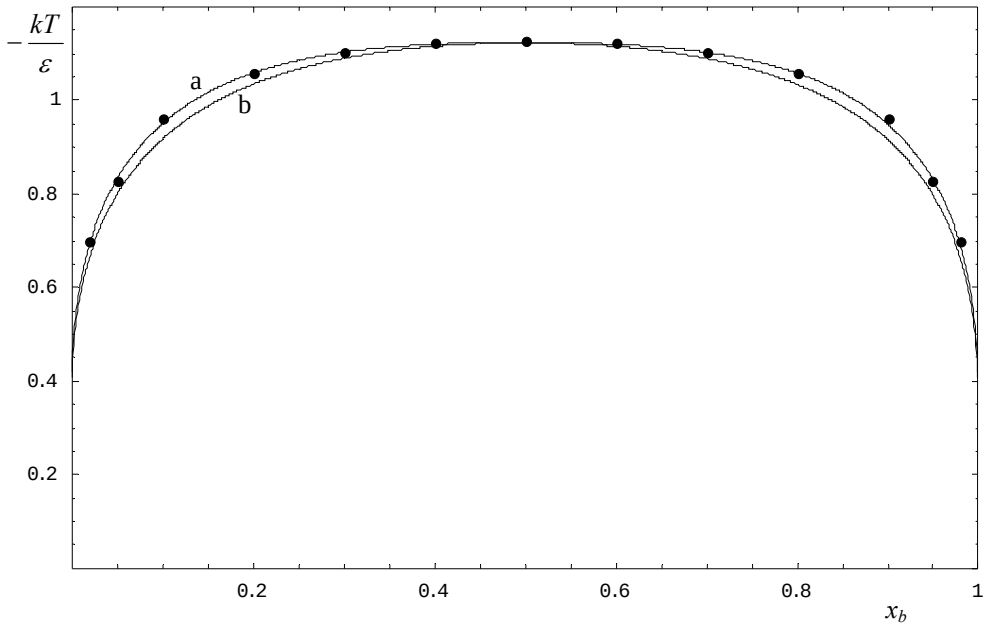

Figure 24. Binodal for three-dimensional (cubic) lattice: (a) - equation (77); (b) - equation (63); solid circles show Monte Carlo simulation data for binodal from ref.[90]. Here $B_b = 2$, and $\nu_b = 0.65$.

a

Papers published during the contract period
and further publications based on results of the contract

1. G.L. Aranovich, and M.D. Donohue, "Phase Loops in Density Functional Theory Calculations of Adsorption in Nanoscale Pores", *Physical Review E* **60**, 5552 (1999).

2. G.L. Aranovich, P.S. Donohue, and M.D. Donohue, "A Lattice Model for Fluids with Directional Interactions", *Journal of Chemical Physics* **111**, 2050 (1999).

3. G.L. Aranovich, and M.D. Donohue, "Adsorption of Chain Molecules", *Journal of Colloid and Interface Science* **213**, 457 (1999).

4. T. Hocker, G.L. Aranovich , and M.D. Donohue. "Monolayer Adsorption for the Subcritical Lattice Gas and Partially Miscible Binary Mixtures", *Journal of Colloid and Interface Science* **211**, 61 (1999).

5. T. Hocker, G.L. Aranovich, and M.D. Donohue, "Monolayer Adsorption of Nonrandom Mixtures", *The Journal of Chemical Physics* **111**, 1240 (1999).

6. D.-W. Wu, G.L. Aranovich, and M.D. Donohue, "Adsorption of Dimers at Surfaces", *Journal of Colloid and Interface Science* **212**, 301 (1999).

7. M.D. Donohue, and G.L. Aranovich, "A New Classification of Isotherms for Gibbs Adsorption of Gases on Solids", *Fluid Phase Equilibria* **158-160**, 557 (1999).

8. G.L. Aranovich, and M.D. Donohue M.D., "Vapor Adsorption on Microporous Adsorbents", *Carbon* **38**, 701 (2000).

9. G.L. Aranovich, C. Sangwichien, and M.D. Donohue, "Intermolecular Repulsions in Adsorbed Layers", *Journal of Colloid and Interface Science* **227**, 553 (2000).

10. G.L. Aranovich, and M.D. Donohue, "Lattice Density Functional Theory Predictions of Order-Disorder Phase Transitions", *Journal of Chemical Physics* **112**, 2361 (2000).

11. D.-W. Wu, G.L. Aranovich, and M.D. Donohue, "Nonrandom Behavior of Amphiphilic Dimers in Solution", *Journal of Chemical Physics* **113**, 3404 (2000).

12. D.-W. Wu, G.L. Aranovich, and M.D. Donohue, "Adsorption of Amphiphilic Dimers at Surfaces", *Journal of Colloid and Interface Science* **230**, 281 (2000).

13. G.L. Aranovich, and M.D. Donohue, "Surface Compression in Adsorption Systems", *Colloids and Surfaces A* **187-188**, 95 (2001).

14. G.L. Aranovich, and M.D. Donohue, "A Simple Lattice Model for Phase Transitions in Block Copolymers", *The Journal of Chemical Physics* **115**, 5331 (2001).

15. M.P. Chernoff, G.L. Aranovich, and M.D. Donohue, "Density Functional Theory Calculations of the Energy and Free Energy of Anisotropic Multicomponent Mixtures", *The Journal of Chemical Physics* **116**, 9395 (2001).

16. T. Hocker, and M.D. Donohue, "A Simple Model for Solute Partitioning and Adsorption, *Journal of Colloid and Interface Science* **244**, 9 (2001).

17. T. Hocker, G.L. Aranovich, and M.D. Donohue, "Adsorption Energy Distribution of Heterogeneous Surfaces Predicted from Projections on Convex Sets", *Journal of Colloid and Interface Science* **238**, 167 (2001).

18. G.L. Aranovich, and M.D. Donohue, "Modeling Self-Assembly in Molecular Fluids", *The Journal of Chemical Physics* **116**, 7255 (2002).

19. C. Sangwichien, G.L. Aranovich, and M.D. Donohue, "Density Functional Theory Predictions of Adsorption Isotherms with Hysteresis Loops", *Colloids and Surfaces A* **206,** 313 (2002).

20. J.S. Erickson, G.L. Aranovich, and M.D. Donohue, "A Simple Model for Ordering in Adsorbed Layers", *Molecular Physics* **100**, 2121 (2002).

21. G.L. Aranovich, and M.D. Donohue, "Adsorption Compression: An Important New Aspect of Adsorption Behavior and Capillarity", *Langmuir* **19**, 2722 (2003).

22. G.L. Aranovich, and M.D. Donohue, "Critical Point Corrections for Equilibrium between Two- and Three-Dimensional Phases", *Langmuir* **19**, 2162 (2003).

23. G.L. Aranovich., and M.D. Donohue, "Phenomenon of Surface Compression", 39th IUPAC Congress Abstracts, Ottawa, 2003, p. 99.

24. G.L. Aranovich, and M.D. Donohue, "Critical Point Corrections for Lattice Systems", *The Journal of Chemical Physics* **119,** 478 (2003).

25. G.L. Aranovich, and M.D. Donohue, "Theory of Multilayer Adsorption with Correct Critical Behavior", *Langmuir* **19**, 3822 (2003).

26. J.S. Erickson, G.L. Aranovich, and M.D. Donohue, "Solution Microstructure of Confined Fluids with Directional Interactions under the Influence of an External Field: Mean Field Considerations", *Molecular Simulation* **30**, 507 (2004).

27. T.E. Wetzel, J.S. Erickson, P.S. Donohue, C.L. Charniak, G.L. Aranovich, and M.D. Donohue, "Monte Carlo Simulations on the Effect of Substrate Geometry on Adsorption and Compression", *The Journal of Chemical Physics* **120**, 11765 (2004).

28. D. Matuszak, G.L. Aranovich, and M.D. Donohue, "Lattice Density Functional Theory of Molecular Diffusion", *The Journal of Chemical Physics* **121**, 426 (2004).

29. G.L. Aranovich, J.S. Erickson, and M.D. Donohue, “Lattice Gas 2D/3D Equilibria: Chemical Potentials and Adsorption Isotherms with Correct Critical Points”, *Journal of Chemical Physics* **120**, 5208 (2004).

30. G.L. Aranovich, and M.D. Donohue, “Diffusion Equation for Interacting Particles”, *Journal of Physical Chemistry B* **109**, 16062 (2005).

31. G.L. Aranovich, and M.D. Donohue, “The Role of Adsorption Compression in Nano-Capillarity”, *Journal of Colloid and Interface Science* **292**, 202 (2005).

32. G.L. Aranovich, T.E. Wetzel, and M.D. Donohue, “Adsorption Behavior of Repulsive Molecules”, *Journal of Physical Chemistry B* **109**, 10189 (2005).

REFERENCES

1. G.L. Aranovich, and M.D. Donohue M.D., *Carbon* **38**, 701 (2000).
2. G.L. Aranovich, C. Sangwichien, and M.D. Donohue, *Journal of Colloid and Interface Science* **227**, 553 (2000).
3. D.P. Valenzuela, and A.L. Myers, Adsorption Equilibrium Data Handbook, Prentice Hall, New Jersey, 1989.
4. S. Sircar and A.L. Myers, *AIChE Journal* **19**, 159 (1973).
5. T. Nakahara, M. Hirata and T. Omori, *J. Chem. Eng. Data* **19**, 310 (1974).
6. O. Talu and I. Zwiebel, *AIChE Journal* **32**, 1263 (1986).
7. S.H. Hyun and R.P. Danner, *J. Chem. Eng. Data* **27**, 196 (1982).
8. J.T. Nolan, T.W. McKeehan and R.P. Danner, *J. Chem. Eng. Data* **26**, 112 (1981).
9. B.K. Kaul, *Ind. Eng. Chem. Res.* **26**, 928 (1987).
10. L. Szepesy and V. Ilies, *Acta Chim. Hung.* **35**, 37 (1963).
11. D.P. Valenzuela and A.L. Myers, Adsorption Equilibrium Data Handbook, Prentice Hall, New Jersey, 1989.
12. G.L. Aranovich and M.D. Donohue, *Colloids and Surfaces A* **187-188**, 95 (2001).
13. G.L. Aranovich, and M.D. Donohue, *Journal of Chemical Physics* **112**, 2361 (2000).
14. G.L. Aranovich, and M.D. Donohue, *Physical Review E* **60**, 5552 (1999).
15. D.-W. Wu, G.L. Aranovich, and M.D. Donohue, "Adsorption of Amphiphilic Dimers at Surfaces", *Journal of Colloid and Interface Science* **230,** 281 (2000).
16. D.-W. Wu, G.L. Aranovich, and M.D. Donohue, "Nonrandom Behavior of Amphiphilic Dimers in Solution", *Journal of Chemical Physics* **113**, 3404 (2000).
17. S.L. Aggarwal, Ed. *Block Copolymers*, Plenum press, New York, 1970.
18. A. Noshay, and J.E. McGrath, Block Copolymers: Overview and Critical Survey, Academic Press, New York, 1979.
19. I.W. Hamley, *Block Copolymers*, Oxford University Press, Oxford, 1999.
20. F.S. Bates, and G.H. Fredrickson, *Physics Today*, February, 1999, p.32-38.
21. D. Zhao, J. Feng, Q. Huo, N. Melosh, G.H. Fredrickson, B.F. Chmelka, and G.D. Stucky, *Science* **279**, 548 (1998).
22. T. Hino, and J.M. Prausnitz, *Macromolecules* **31**, 2636 (1998).
23. C.C. Lin, S.V. Jonnalagadda, P.K. Kesani, H.J. Dai, and N.P. Balsara, *Macromolecules* **27**, 7769 (1994).
24. G.L. Aranovich, and M.D. Donohue, *Computers & Chemistry* **22**, 429 (1998).
25. G.L. Aranovich, and M.D. Donohue, *Physical Review E* **60**, 5552 (1999).
26. G. M. Martinez, *J. Chem. Phys.* **103**, 9813 (1995).
27. L. Leibler, *Macromolecules* **13**, 1602 (1980).
28. D.A. Young, *J. Chem. Phys.* **58 (4)**, 1647 (1973).
29. A.R. Denton, and N.W. Ashcroft, *Phys. Rev. A* **42**, 7312 (1990).
30. X.C. Zeng, and D.W. Oxtoby, *J. Chem. Phys.* **93**, 2692 (1990); **93**, 4357(1990).
31. C. Vega, E.P.A. Paras, and P.A. Monson, *J. Chem. Phys.* **97 (11)**, 8543 (1992).
32. P. Bolhuis, and D. Frenkel, *Phys. Rev. Letters* **72(14)** 2211 (1994).
33. D.A. Kofke, *Phys. Rev. E* **59(1)** 618 (1999).
34. C. Vega, E.P.A. Paras, and P.A. Monson, *Mol. Phys.* **77**, 803 (1992).
35. W.G. Hoover, and F. Ree, *J. Chem. Phys.* **49**, 3609 (1968).
36. J.A. Barker, *J. Chem. Phys.* **44**, 4212 (1966).

37. D. Henderson, and J.A. Barker, *Mol. Phys.* **14**, 587 (1968).
38. J.A. Barker, *J. Chem. Phys.* **63**, 632 (1975).
39. A.D.J. Haymet, *Annu. Rev. Phys. Chem.* **38**, 89 (1987);
M. Baus, *J. Stat. Phys.* **48**, 1129 (1987);
M. Baus, *J. Phys. Condensed Matter* **2**, 2111 (1990).
40. P. Tarazona, *Phys. Rev. A* **31**, 2672 (1985).
41. G.L. Aranovich, and M.D. Donohue, *Phys. Rev. E* , **60**, 5552 (1999).
42. N.A. Modine, G. Zumbach, and E. Kaxiras, *Phys. Rev.* B **55**, 10289 (1997).
43. W.G. Kranedonk, and D. Frenkel, *Mol. Phys.* **72**, 679 (1991).
D. Kofke, *Mol. Simul.* **7**, 285 (1991).
44. C.N. Yang, and T.D. Lee, *Phys. Rev.* **87**, 410 (1952).
45. L.K.Runnels, Lattice Gas Theories of Melting, In: *Phase Transitions and Critical Phenomena*, Ed. by G. Domb and M.S. Green, vol. 3, Academic Press, NY, 1972, p.305-329.
46. F.H. Ree, and D.A. Chesnut, *Phys. Rev. Letters* **18**, 5 (1967).
47. L.K. Runnels, J.P.Salvant, and H.R. Streiffer, *J. Chem. Phys.* **52**, 2352 (1970).
48. B. Widom, and J.S. Rowlinson, *J. Chem. Phys.* **52**, 1670 (1970).
49. J.L. Lebowitz, A. Mazel, P. Nielaba, and L. Samaj, *Phys. Rev. E* **52 (6)**, 5985 (1995).
50. B.R. Riemenschneider, and D.A. Huckaby, *J. Chem. Phys.* **58**, 3940 (1973).
51. D.A. Huckaby, *Phys. Rev. B* **20 (3)**, 1208 (1979).
52. D.A. Huckaby, *J. Stat. Phys.* **33 (1)**, 23 (1983).
53. D.A. Huckaby, *Lecture Notes in Physics* **206**, 290 (1984).
54. Y. Cui, C.M. Lieber, *Science* **291**, 851 (2001).
55. A.W. Oslen, Z.H. Kafafi, *J. Amer. Chem. Soc.* **113**, 7758 (1991).
56. M.W. Matsen, F.S. Bates, *Macromolecules* **29**, 7641 (1996).
57. Z. Gao, K.S. Siow, H.S.O. Chan, *Synthetic Metals* **75**, 5 (1995).
58. J. Joo, A.J. Epstein, *Appl. Phys. Lett.* **65**, 2278 (1994).
59. R.H. Baughman, *Synthetic Metals* **78**, 339 (1996).
60. J.L. Cuichard, A Mocellin, M.O. Simonnot, J.F. Remy, M. Sardin, *Powder Technology* **99**, 257 (1998).
61. M.J. Mayo, *International Materials Reviews* **41**, 85 (1996).
62. T. Hirano, W. Li, L. Abrams, P.J. Krusic, M.F. Ottaviani, N.J. Turro, *J. Org. Chem.* **65**, 1319 (2000).
63. A. Shiloach, D. Blankschtein, *Langmuir* **14**, 1618 (1998).
64. Merriam-Webster's Collegiate Dictionary (Marriam-Webster, Inc., Springfield, Massachusetts, 2001).
65. G. L. Aranovich and M. D. Donohue, *J. Chem. Phys.* **105**, 7059 (1996).
66. J. H. Hildebrand, *J. Am. Chem. Soc.* **51**, 66 (1929).
67. Anisimov, M.A.; Povodyrev, A.A.; Kulikov, V.D.; Sengers, J.V. *Phys. Rev. Letters* **1995**, 75, 3146.
68. Anisimov, M.A.; Kiselev, S.B.; Sengers, J.V. *Physica A* **1992**, 188, 487.
69. Chakraborty, A.K.; Golumbfskie, A.J. *Annu. Rev. Phys. Chem.* **2001**, 52, 537.
70. Russel, W.B.; Saville, D.A.; Schowalter, W.R. *Colloidal Dispersions*; Cambridge University Press: New York, 1989.

71. Gale, P.A. *Phil. Trans. R. Soc. London A* **2000**, 358, 431.
72. Kiely, C.J.; Fink, J.; Brust, M.; Bethell, D.; Schiffrin, D.J. *Nature* **1998**, 396, 444.
73. Aranovich, G.L.; Donohue, M.D. *J. Chem. Phys.* **2002**, 116, 7255.
74. Aranovich, G.L.; Donohue, M.D. *J. Chem. Phys.* **2001**, 115, 5331.
75. Aranovich, G.L.; Hocker, T.; Wu, D.-W.; Donohue, M.D. *J. Chem. Phys.* **1997**, 106, 10282.
76. Ono, S.; Kondo, S. *Molecular Theory of Surface Tension in Liquids*, In: *Encyclopedia of Physics* (ed. S. Flügge); Springer: Berlin, 1960; vol.10, p. 134.
77. Rowlinson, J.S.; Widom, B. *Molecular Theory of Capillarity*; Clarendon Press: Oxford, 1982.
78. Lane, J.E. in *Adsorption from Solution at a Solid/Liquid Interface*, ed. by G. Parfitt and C. Rochester; sect. 3; Academic Press: London, 1983;
79. Lane,J.E.; Johnson, C.H.J. *Aust. J. Chem.* **1967**, 20, 611.
80. Aranovich, G.L. *Langmuir* **1992**, 8, 736.
81. Hocker, T.; Aranovich, G.L.; Donohue, M.D. *J. Chem. Phys.* **1999**, 111, 1240.
82. Altenberger, A.R.; Stecki, J. *Chem. Phys. Letters* **1970**, 5, 29.
83. Yashonath, S; Sarma, D.D. *Chem. Phys. Letters* **1984**, 110, 265.
84. Aranovich, G.L.; Donohue, M.D. *Physical Review E* **1999**, 60, 5552.
85. Aranovich, G.L.; Donohue, M.D. *Computers & Chemistry* **1998**, 22, 429.
86. De Oliveira, M.J.; Griffiths, R.B. *Surface Science* **1978**, 71, 687.
87. Wagner, P.; Binder, K. *Surface Science* **1986**, 175, 421.
88. Aranovich, G.L.; Donohue, M.D. *Journal of Colloid and Interface Science* **1997**, 189, 101.
89. Hill, T.L. *An Introduction to Statistical Thermodynamics,* Addison-Wesley: London, 1960.
90. Lambert, S.M.; Soane, D.S.; Prausnitz, J.M. *Fluid Phase Equilibria* **1993**, 83, 59.
91. Masel, R. *Principles of Adsorption and Reaction on Solid Surfaces*, section 4.8.1; John Wiley: New York, 1996.